Atmos. Chem. Phys., 24, 12881–12901, 2024
https://doi.org/10.5194/acp-24-12881-2024

Atmospheric Chemistry and Physics
Open Access
EGU

Research article

Understanding the mechanism and importance of brown carbon bleaching across the visible spectrum in biomass burning plumes from the WE-CAN campaign

Yingjie Shen[1], Rudra P. Pokhrel[1,a], Amy P. Sullivan[2], Ezra J. T. Levin[2,b], Lauren A. Garofalo[3], Delphine K. Farmer[3], Wade Permar[4], Lu Hu[4], Darin W. Toohey[5], Teresa Campos[6], Emily V. Fischer[2], and Shane M. Murphy[1]

[1]Department of Atmospheric Science, University of Wyoming, Laramie, WY 82071, USA
[2]Department of Atmospheric Science, Colorado State University, Fort Collins, CO 80523, USA
[3]Department of Chemistry, Colorado State University, Fort Collins, CO 80523, USA
[4]Department of Chemistry and Biochemistry, University of Montana, Missoula, MT 59812, USA
[5]Department of Atmospheric and Oceanic Sciences, University of Colorado Boulder, Boulder, CO 80309, USA
[6]National Center for Atmospheric Research, Atmospheric Chemistry Division, Boulder, CO 80301, USA
[a]now at: Air Pollution Control Division, Colorado Department of Public Health and Environment, Denver, CO 80246, USA
[b]now at: METEC Research Group, Colorado State University Energy Institute, Fort Collins, CO 80524, USA

Correspondence: Shane M. Murphy (shane.murphy@uwyo.edu)

Received: 22 December 2023 – Discussion started: 18 January 2024
Revised: 16 September 2024 – Accepted: 23 September 2024 – Published: 21 November 2024

Abstract. Aerosol absorption of visible light has an important impact on global radiative forcing. Wildfires are one of the major sources of light-absorbing aerosol, but there remains significant uncertainty about the magnitude, wavelength dependence, and bleaching of absorption from biomass burning aerosol. We collected and analyzed data from 21 western US wildfire smoke plumes during the 2018 Western Wildfire Experiment for Cloud Chemistry, Aerosol Absorption and Nitrogen (WE-CAN) airborne measurement campaign to determine the contribution of black carbon (BC), brown carbon (BrC), and lensing to the aerosol mass absorption cross section (MAC). Comparison to commonly used parameterizations and modeling studies suggests that model overestimation of absorption is likely due to incorrect BrC refractive indices. Modelers (Wang et al., 2018; Carter et al., 2021) invoke a bleaching process that decreases the MAC of organic aerosol (OA) to offset the overestimation of absorption in models. However, no evidence of a decreasing MAC is observed in individual WE-CAN fire plumes or in aged plumes from multiple fires. A decrease in OA mass and water-soluble organic carbon (WSOC), both normalized by carbon monoxide (CO) to correct for dilution, is observed with an increasing oxygen-to-carbon (O : C) ratio and a decreasing gas-phase toluene : benzene ratio, when data from all fires are combined in half of the individual fire plumes. This results in a strong decrease in total absorption at 405 nm and a slight decrease at 660 nm with these chemical markers. These results demonstrate that changes in absorption with chemical markers of plume age are the result of decreasing OA rather than changes in the MAC of the organic material itself. While decreasing MAC or OA mass with aging could both be called bleaching and can both correct overestimation of absorption in models, it is important to distinguish between these two effects because decreasing OA mass will also decrease scattering, which will cause a significantly different net radiative effect. We also find that an average of 54 % of non-BC absorption (23 % total absorption) at 660 nm is from water-soluble BrC, confirming that BrC absorption is important across the visible spectrum. Quantification of significant BrC at red wavelengths and observation of bleaching being caused by changes in OA with O : C and toluene : benzene markers of plume age provide important improvements to our understanding of BrC and critical constraints on aerosol absorption in regional and global climate models.

Published by Copernicus Publications on behalf of the European Geosciences Union.

1 Introduction

Atmospheric aerosol impacts the climate system by directly scattering and absorbing solar radiation, by indirectly changing cloud properties, and by deposition that changes surface albedo (McConnell et al., 2007; Sarangi et al., 2020). Biomass burning injects a large amount of primary organic aerosol (POA), secondary organic aerosol (SOA), and black carbon (BC) into the atmosphere every year. BC is somewhat poorly defined but is generally considered to be insoluble, be refractory, and have an absorption exponent near 1. Other materials such as elemental carbon (EC) and soot (Wei et al., 2013) are often very similar to BC, but each is operationally defined by how it is measured. Although it only represents a small fraction of aerosol mass, BC has a significant impact on the global energy budget due to its ability to strongly absorb solar radiation at all visible wavelengths. While still important, positive radiative forcing of BC is lower in IPCC AR6 (2022) than in IPCC AR5 (2013). Bond et al. (2013) estimated the direct radiative forcing for BC from 1750 to 2005 at the top of the atmosphere (TOA) to be $+0.71\,\mathrm{W\,m^{-2}}$, with an uncertainty of 90 %, while the latest IPCC AR6 (2022) estimates the effective radiative forcing for BC from 1750 to 2019 to be $+0.11$ (-0.2 to $+0.42$) $\mathrm{W\,m^{-2}}$. It is important to note that AR5 reported direct radiative forcing, while AR6 reports effective radiative forcing. While BC is emitted from nearly all combustion processes, the largest global source of BC is thought to be biomass burning (Bond et al., 2013). Organic aerosol (OA) also absorbs visible light, but its absorption strongly depends on the wavelength of light (Kirchstetter et al., 2004). Non-BC light-absorbing organic compounds are often called brown carbon (BrC), and they are usually co-emitted with BC or formed by secondary chemistry in biomass burning plumes (Andreae and Gelencsér, 2006). Unlike BC, which absorbs light from the UV to the IR, BrC absorption sharply increases in the UV and shorter visible portions of the spectrum and has historically been considered to be almost transparent near the red wavelengths (Andreae and Gelencsér, 2006; Bahadur et al., 2012; Liu et al., 2020). The global-mean TOA direct radiative forcing from BrC also shows large uncertainty, with estimates ranging from $+0.03$ to $+0.57\,\mathrm{W\,m^{-2}}$ (Saleh, 2020). Wildfires in the western US have increased in recent decades (Westerling et al., 2006; Burke et al., 2021) and will continue increasing according to model predictions (Yue et al., 2013; Hurteau et al., 2014; Ford et al., 2018; Neumann et al., 2021). Therefore, quantitative studies of the radiative effects caused by BC and BrC emitted from wildfires are crucial for a better understanding of future climate and are essential for improving climate models.

The high uncertainty in the radiative forcing from BC is caused by both uncertainties in emissions and uncertainty in the properties that affect its optics, such as size distribution, morphology, refractive index, and mixing state (Bond et al., 2006; Kleinman et al., 2020; Brown et al., 2021). For wildfires, most of the aerosol mass is organic (Garofalo et al., 2019). When BC is internally mixed with OA, it is coated by other absorbing or non-absorbing materials that cause more photons to interact with the BC core and therefore enhance the absorption of the BC core. This process is often called the lensing effect, even though geometric lensing is not actually happening at these sizes (Fuller and Kreidenweis, 1999). The absorption enhancement caused by the lensing effect is defined as the ratio of the absorption cross section of a coated BC particle to that of an equivalent uncoated BC particle (Lack and Cappa, 2010). Laboratory experiments have shown a strong absorption enhancement of BC by a factor of 2 or more (Schnaiter et al., 2003, 2005; Bond and Bergstrom, 2006; Bond et al., 2006; Peng et al., 2016). Observations of absorption enhancement from ambient BC vary widely in field studies due to variations in coating thickness, coating material, source type, or methodological differences, but this is often much lower than laboratory values (Liu et al., 2015, 2017; Cappa et al., 2012, 2019; Healy et al., 2015; Krasowsky et al., 2016). Cappa et al. (2019) summarized absorption enhancements observed at the red end of the visible spectrum from 10 studies including ambient measurements, source sampling, and laboratory experiments. The absorption enhancement reported by those measurements ranged from 1.1 to 2.8. Lack and Cappa (2010) found that the absorption enhancement caused by the absorbing shell would be smaller than the absorption enhancement caused by the pure scattering shell. The nonspherical morphology of BC and the tendency of BC to compact when coated by organics can also both enhance and decrease absorption (Romshoo et al., 2021; Kelesidis et al., 2022).

The mass absorption cross section of BC ($\mathrm{MAC_{BC}}$) is an alternative method to quantify the absorbing ability of BC-containing particles compared to absorption enhancement. By describing the absorption per unit mass of BC, $\mathrm{MAC_{BC}}$ can be a fundamental input in climate models to convert mass concentration into absorption coefficients (Cho et al., 2019). $\mathrm{MAC_{BC}}$ is the particulate absorption divided by the mass of the pure BC at a certain wavelength. In this way, the calculated $\mathrm{MAC_{BC}}$ will include absorption of the BC core along with the absorption and absorption enhancement caused by the coating material. Unfortunately, the MAC of the overall BC particle, $\mathrm{MAC_{BC}}$, in the ambient atmosphere continues to be poorly understood due to a lack of field measurements and limitations of filter-based instruments in measuring this parameter. Processes that occur during atmospheric aging of BC also introduce uncertainties into its absorption. Bond and Bergstrom (2006) suggested a $\mathrm{MAC_{BC}}$ of $7.5 \pm 1.2\,\mathrm{m^2\,g^{-1}}$ at 550 nm for fresh BC. The following campaigns demonstrate the variety of $\mathrm{MAC_{BC}}$ measured in the ambient during the past 15 years. Subramanian et al. (2010) reported $\mathrm{MAC_{BC}}$

values of $10.9 \pm 2.1\,m^2\,g^{-1}$ at 660 nm and $13.1\,m^2\,g^{-1}$ at 550 nm over Mexico City when using the Single Particle Soot Photometer (SP2) and the filter-based Particle Soot Absorption Photometer (PSAP) for airborne measurements. Krasowsky et al. (2016) reported a MAC_{BC} enhancement of 1.03 ± 0.05 due to the coatings on BC. Zhang et al. (2017) found a MAC_{BC} with a mean of $10\,m^2\,g^{-1}$ and a standard deviation of $4\,m^2\,g^{-1}$ at 660 nm using both SP2 and PSAP measurements. Cho et al. (2019) summarized the MAC_{BC} estimated from more than 10 studies in East and South Asia under both ambient conditions and in laboratory experiments, and the values ranged from 4.6 to $11.3\,m^2\,g^{-1}$.

The limitations of current measurement techniques bring major uncertainty when quantifying BrC absorption, because BrC is usually co-emitted with BC, which makes it challenging to measure BrC absorption independently. BrC absorption can be measured directly through the solvent-extraction method (Peltier et al., 2007; Zeng et al., 2021; Sullivan et al., 2022) or a thermodenuder (Cappa et al., 2012; Liu et al., 2015; Pokhrel et al., 2017). However, the solvent-extraction method will miss BrC that is insoluble in water or organic solvents, and thermal denuders miss BrC that is not volatile at the denuder temperature. BrC absorption can also be calculated from multiwavelength total absorption measurements, but this approach must assume the absorption Ångström exponent (AAE) for BC and assumes that BrC does not absorb at longer wavelengths, adding significant uncertainty.

To improve our understanding of the evolution of light-absorbing aerosol from biomass burning, smoke from 21 wildfires in the western US was measured near their sources and downwind on board the NSF/NCAR C-130 aircraft during the Western Wildfire Experiment for Cloud Chemistry, Aerosol Absorption and Nitrogen (WE-CAN) campaign. This campaign represented an airborne attempt to fully characterize western US wildfires from several different fuel types, locations, and fire stages (flaming and smoldering). This paper presents novel observations of the absorbing properties of the aerosol and compares these observations to modeling studies conducted with the WE-CAN data and to results from the Fire Influence on Regional to Global Environment – Air Quality (FIREX) study conducted in 2019 (Zeng et al., 2021).

2 Experimental method

This work relies on measurements made during the WE-CAN field campaign, which sampled smoke emitted by wildfires across the western US using the NSF/NCAR C-130 research aircraft. The goal of the campaign was to make detailed observations of the physical, chemical, and optical evolution of aerosol in western wildfire smoke and its impact on climate, air quality, weather, and nutrient cycles. The WE-CAN field campaign consisted of 19 research flights that took place from 24 July to 13 September 2018. Data from 13 flights where all the required instrumentation was available were analyzed in this study. The flight path and dominant wildfire for each of these flights are shown in Fig. 1. The fire locations and fuel types for each fire during WE-CAN were characterized and summarized by Lindaas et al. (2021).

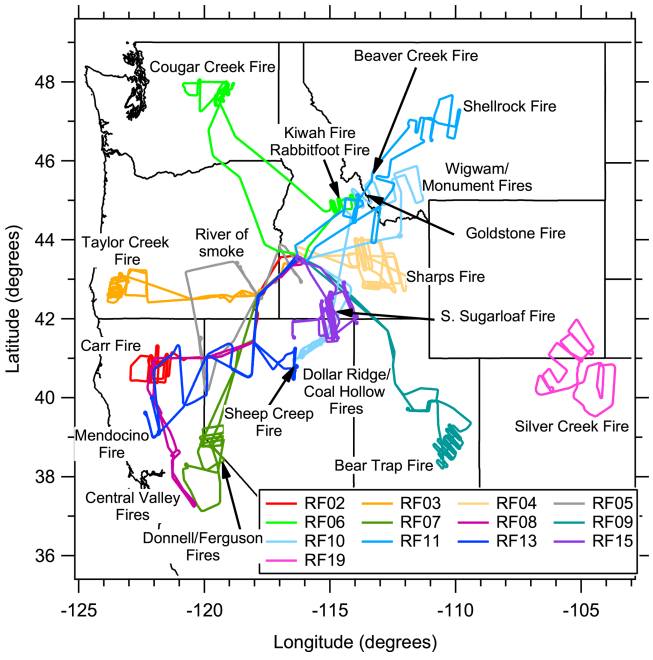

Figure 1. Flight paths and the sampled wildfires for the WE-CAN flights analyzed in this paper.

2.1 Instrumentation

The following instruments are a subset of those flown during the WE-CAN campaign and are utilized in this work. The full WE-CAN dataset is archived at https://data.eol.ucar.edu/master_lists/generated/we-can (last access: 4 May 2021). All the aerosol instruments utilized in this paper, except for the Particle-into-Liquid Sampler (PILS), pulled air from the same Solid Diffuser Inlet (SDI). PILS sampled from a Submicron Aerosol Inlet (SMAI) (Craig et al., 2013a, b, 2014; Moharreri et al., 2014). To eliminate artificial differences in the measurements that would arise from different instruments having different pressures and temperatures after the inlets, all data were converted to either mixing ratio or standard temperature and pressure (STP) conditions (1 atm, 0 °C). Converting to STP has an additional benefit over converting to ambient conditions in that, similar to the mixing ratio, aerosol mass concentrations ($\mu g\,m^{-3}$) and aerosol optical properties (Mm^{-1}) converted to STP stay constant with altitude unless there is a chemical or physical change beyond parcel expansion. Because of this, conversion to STP also allows for division of mass concentrations and optical properties by mixing ratios. All the WE-CAN measurements were converted to STP based on the measured inlet tempera-

ture and pressure (Eq. 1) before data were uploaded, and they have been used in other papers from WE-CAN (Palm et al., 2020; Sullivan et al., 2022).

$$\text{Variables}_{\text{STP}} = \text{Variables}_{\text{measured}} \cdot \frac{\text{Pressure}_{\text{STP}}}{\text{Pressure}_{\text{measured}}} \cdot \frac{\text{Temperature}_{\text{measured}}}{\text{Temperature}_{\text{STP}}} \quad (1)$$

2.1.1 Photoacoustic Absorption Spectrometer (PAS)

Aerosol absorption coefficients were measured with the multiwavelength PAS built by the University of Wyoming (Foster et al., 2019), based on the design of Lack et al. (2012b). A PAS can directly measure the absorption coefficient of dry aerosol. It represents the only way to directly measure aerosol absorption other than with a photothermal interferometer (PTI; Sedlacek and Lee, 2007), which measures the change in the refractive index of the air near particles caused by heating from absorption. Briefly, when modulated laser light (at the resonant frequency of the cell) is absorbed by the aerosol, it heats the surrounding air, inducing pressure waves that are amplified by the cavity and then detected by two microphones (Lack et al., 2006; Foster et al., 2019). The PAS used here has four cells that measure the aerosol absorption coefficient from dry air at 405 and 660 nm and thermally denuded air at 405 and 660 nm. The denuder was set to 300 °C, with the goal of evaporating volatile organic aerosol, which might have a potential impact on light absorption. However, absorption from the denuded channels was not used in this study, because the absorption enhancement calculated using the thermodenuder approach was much smaller than the approach of taking the ratio of MAC_{BC} to $MAC_{BC\text{-}core}$, and we believe that the discrepancy is due to the presence of significant residual organic material after denuding. Two NO_x denuders coated with potassium hydroxide, guaiacol, and methanol were installed on the PAS in front of the inlet to remove the absorption from gas-phase NO_2 (Williams and Grosjean, 1990). No evidence of NO_2 absorption (which would cause baseline shifts) was observed during filter measurements, which are acquired every few minutes. A 3 L min^{-1} $PM_{2.5}$ cyclone (URG-2000-30ED) was used on the PAS in front of the inlet to provide a $PM_{1.0}$ cut at a total flow rate of 5.7 L min^{-1}. In addition, a Nafion drier (Purma Pure PD-100T-24MPS) with 100 tubes was installed on the inlet system to dry-sample to a relative humidity below 30 %. The particle loss (< 3 %) in the drier was corrected during postprocessing. The uncertainty in the absorption coefficient measured by the PAS mainly comes from the calibration technique, in which the highly absorbing substance Regal Black and the Cavity-Attenuated Phase Shift Spectrometer (CAPS) PM_{SSA} were utilized (Foster et al., 2019). The PAS was routinely calibrated (after each flight or every other day if there was a flight every day) during WE-CAN with an accuracy of ±10 %.

The PAS microphone shows a pressure-dependent response to pressure. To account for this behavior, we performed pressure-dependent calibration of the PAS where the instrument pressure (both PAS and CAPS PM_{SSA}) was dropped stepwise by ∼ 50 torr from the ambient to ∼ 300 torr (typical minimum pressure level during WE-CAN). A calibration was performed at each pressure step, and the calibration constants were fitted with pressure to get a change in calibration at a desired pressure. Pressure-dependent calibrations were repeated pre and post campaign to capture variability.

2.1.2 CAPS PM_{SSA}

After pulling through the NO_x denuder, the $PM_{1.0}$ cyclone, and the Nafion drier in front of the PAS inlet, the sampled air entered through the Aerodyne CAPS PM_{SSA_450} and CAPS PM_{SSA_660} to measure the aerosol scattering and extinction coefficients at 450 and 660 nm, respectively. CAPS PM_{SSA} instruments measure extinction by utilizing cavity-attenuated phase shift spectroscopy and measure scattering with an integrating sphere (Onasch et al., 2015). Ammonium sulfate particles were used to calibrate the scattering channel of the CAPS PM_{SSA} during WE-CAN with an accuracy of ±3 %.

2.1.3 PILS system

BrC absorption and water-soluble organic carbon (WSOC) were measured using the PILS system (Sullivan et al., 2022). PILS continuously collects ambient particles into purified water and provides a liquid sample with the aerosol particles dissolved in it for analysis (Orsini et al., 2003). The size cut for PILS was provided by a non-rotating micro-orifice uniform deposit impactor (MOUDI) with a 50 % transmission efficiency of 1 µm (aerodynamic diameter) at 1 atmosphere ambient pressure (Marple et al., 1991). The total air flow for PILS was approximately 15 L min^{-1}. Upstream of PILS was an activated carbon parallel-plate denuder (Eatough et al., 1993) to remove organic gases. In addition, a valve was periodically closed manually for 10 min, diverting the air flow through a Teflon filter before entering PILS and allowing for background measurements. The liquid sample obtained from PILS was pushed through a 0.2 µm PTFE liquid filter using a set of syringe pumps to ensure that insoluble particles were removed. The flow was then directed through a liquid waveguide capillary cell (LWCC) and a total organic carbon (TOC) analyzer for near-real-time measurement of BrC absorption and WSOC, respectively. More details and a schematic illustration can be found in Zeng et al. (2021).

For the absorption measurement, a 2.5 m path-length LWCC (World Precision Instruments, Sarasota, FL) was used. A dual deuterium and tungsten halogen light source (DH-mini, Ocean Optics, Largo, FL) and an absorption spectrometer (FLAME-T-UV-VIS, Ocean Optics, Largo, FL) were coupled to the LWCC via fiber optic cables. Absorp-

tion spectra were recorded using OceanView spectroscopy software over a range from 200 to 800 nm. The wavelength-dependent absorption was calculated following the method outlined in Hecobian et al. (2010). For this study, a 16 s integrated measurement of absorption with a limit of detection (LOD) of 0.1 Mm^{-1} was made (Sullivan et al., 2022).

For the WSOC measurement, a Sievers Model M9 Portable TOC Analyzer (Suez Waters Analytical Instruments, Boulder, CO) was used. This analyzer works by converting the organic carbon in the liquid sample to carbon dioxide through chemical oxidation involving ammonium persulfate and ultraviolet light. The carbon dioxide formed was then measured by conductivity. The increase in the conductivity observed was proportional to the amount of organic carbon in the liquid sample. The analyzer was run in turbo mode, providing a 4 s integrated measurement of WSOC with a LOD of 0.1 µg C m^{-3} (Sullivan et al., 2022).

2.1.4 SP2

Refractory black carbon (rBC) number and mass concentrations were measured with the SP2 (Droplet Measurement Technologies), which uses a continuous, 1064 nm Nd:YAG laser to heat absorbing material, primarily rBC, to its vaporization temperature and measures the resulting incandescence (Schwarz et al., 2006). Similar to the CAPS PM_{SSA}, the sampled air was sent through the NO_x denuder, $PM_{1.0}$ cyclone, and Nafion drier in front of the PAS inlet before it went to the SP2. The SP2 was calibrated with polystyrene latex (PSL) particles and size-selected fullerene soot. On the C-130, the SP2 sample line was diluted with high-efficiency particulate air (HEPA)-filtered, pressured ambient air that was passed through a mass flow controller to prevent signal saturation. During postprocessing the data were corrected for dilution back to ambient concentrations.

2.1.5 Ultra-High Sensitivity Aerosol Spectrometer (UHSAS)

Particle number concentration was measured using a rack-mounted UHSAS. The flow rate of the rack-mounted UHSAS can be manually lowered by the in-flight operator when the aircraft flies across smoke plumes, so that the UHSAS can stay within its optimum concentration measurement range (Sullivan et al., 2022). The UHSAS was calibrated with ammonium sulfate. The particle mass concentration was calculated by applying these size bins and multiplying them by a particle density of 1.4 g cm^{-3} (Sullivan et al., 2022). The volume mean diameters of the particles for all the detected plumes range between 0.18 and 0.34 µm.

2.1.6 Proton-Transfer-Reaction Time-of-Flight Mass Spectrometer (PTR-ToF-MS)

The University of Montana PTR-ToF-MS 4000 (Ionicon Analytik) was utilized to report the volatile organic compound (VOC) mixing ratios during WE-CAN (Permar et al., 2021). Only the toluene and benzene mixing ratios derived from the PTF-ToF-MS were used in this work; their overall uncertainty is < 15 %. More details of the operation, calibration, and validation of the PTR-ToF-MS during WE-CAN can be found in Permar et al. (2021).

2.1.7 High-resolution aerosol mass spectrometry (HR-AMS)

OA was detected using HR-AMS (Aerodyne Inc.). A description of the AMS operation during WE-CAN can be found in Garofalo et al. (2019). The atomic oxygen-to-carbon ratio (O : C) and organic-mass-to-organic-carbon ratio (OM : OC) used in this work were determined using the improved ambient elemental analysis method for AMS (Canagaratna et al., 2015). Average (integrated) elemental ratios were obtained by averaging (integrating) elemental masses of carbon, hydrogen, and oxygen and recalculating elemental ratios.

2.1.8 Quantum cascade laser (QCL) and Picarro cavity ring-down spectrometer

The carbon monoxide (CO) mixing ratio was measured using both an Aerodyne quantum cascade laser instrument (CS-108 miniQCL) and a Picarro cavity ring-down spectrometer (G2401-m WS-CRD) (Garofalo et al., 2019). Because the QCL has better precision than the Picarro instrument, CO measurements from the QCL were preferentially used. However, CO measurements from the Picarro CO data were used for RF10 and RF13, because the CO QCL was not operated during these two flights. The carbon dioxide (CO_2) mixing ratio was also determined from Picarro.

2.2 Plume physical age

The physical age of the plume was calculated by dividing the distance the plume was sampled from the fire source by the in-plume average wind speed. The average wind speed was measured on the NSF/NCAR C-130 aircraft during each plume pass. The distance was estimated by using the longitude and latitude of the geometric center of the plume measured on the NSF/NCAR C-130 and the fire location provided by the U.S. Forest Service. The same method was used by Garofalo et al. (2019), Peng et al. (2020), Lindaas et al. (2021), Permar et al. (2021), and Sullivan et al. (2022) and is also utilized here for consistency.

2.3 Plume-integration method

During the WE-CAN campaign, both the SP2 and PILS had significant hysteresis compared to other instruments. In the SP2 this is because the sampled air was diluted with particle-free ambient air at various ratios to prevent signal saturation. In PILS this is because of the retention effect of liquid on the wetted component or within dead volumes (Zeng et al., 2021). Therefore, it was most accurate to integrate properties across airborne transects of wildfire plumes to avoid the impact of instrument hysteresis and measurement noise, which can dramatically impact instantaneous ratios. Pseudo-Lagrangian sampling was used during the flights for the WE-CAN campaign: the C-130 aircraft repeatedly crossed the smoke plume from a particular fire by traveling perpendicular to the prevailing winds, crossing the plume, turning, and then crossing the plume again further downwind. In this work, we manually identified plume edges based on the inflection point when CO concentrations stopped rapidly changing as we entered and exited the smoke plume. The outsides of the plume measurement periods had CO mixing ratios from 100 to 300 ppbv. The lowest 10 % of each variable from the outside plume segments was set to the background of that variable. If the time between two consecutive outside plume segments was longer than 20 s and the highest CO mixing ratio was 100 ppbv higher than the outside plume CO criteria, this segment was chosen as a plume. The start and end points of each plume were slightly adjusted manually based on the CO mixing ratio to make sure the entire plume was covered. Different start and end points for the SP2 and PILS were adjusted manually based on the rBC mass concentrations and WSOC, respectively.

2.4 Absorption enhancement and mass absorption cross section

Absorption enhancement (E_{abs}) is the ratio of the absorption of all particles (including BC core and coating materials) to the absorption of BC alone (Lack and Cappa, 2010). E_{abs} at 660 nm (E_{abs_660}) was calculated in this study using Eq. (2):

$$E_{abs\_660} = \frac{Abs_{Total\_660}}{M_{BC} \cdot MAC_{BC\_core\_660}}, \quad (2)$$

where Abs_{Total_660} is the total absorption coefficient at a wavelength of 660 nm measured by the PAS, M_{BC} is the mass concentration of BC measured by the SP2, and $MAC_{BC\_core\_660}$ is the MAC of BC alone (without any other coating material) at 660 nm, which is set to 6.3 $m^2\ g^{-1}$ (Bond and Bergstrom, 2006; Subramanian et al., 2010).

The MAC_{BC} at 660 nm was calculated using Eq. (3):

$$MAC_{BC660} = \frac{Abs_{Total\_660}}{M_{BC}}. \quad (3)$$

MAC_{BC660} is utilized more often in this study than E_{abs_660} because there is no widely accepted MAC for BC emitted from wildfires. The MAC of BrC and lensing is calculated at 405 and 660 nm (Eq. 4):

$$MAC_{BrC+lensing\_\lambda} = \frac{Abs_{Total\_\lambda} - M_{BC} \cdot MAC_{BC\_core\_\lambda}}{M_{OA}}, \quad (4)$$

where M_{OA} is the organic mass measured by AMS. Again, the $MAC_{BC\_core\_\lambda}$ is set to 6.3 and 10.2 $m^2\ g^{-1}$, respectively, at 660 and 405 nm, yielding an AAE (the negative slope of a logarithmic absorption coefficient against wavelength) of 0.99 for the BC core (Bond and Bergstrom, 2006; Subramanian et al., 2010; Liu et al., 2015). It should be noted that both BrC and lensing contribute to the $MAC_{BrC+lensing\_\lambda}$ and cannot be separated using this approach, and $MAC_{BrC+lensing\_\lambda}$ is the MAC of all organics without distinguishing between absorbing and non-absorbing particles.

The MAC of water-soluble BrC at λ nm ($MAC_{ws\_BrC\lambda}$) is calculated using Eq. (5):

$$MAC_{ws\_BrC\lambda} = \frac{Abs_{ws\_BrC\lambda}}{WSOC \cdot (WSOM : WSOC)}, \quad (5)$$

where $Abs_{ws\_BrC\lambda}$ is water-soluble light absorption coefficient at λ nm and WSOC is water-soluble organic carbon mass, which are both measured by PILS. The WSOM : WSOC ratio is set to 1.6 (Sullivan et al., 2022). $MAC_{ws\_BrC\lambda}$ is the MAC of all water-soluble organics without distinguishing between absorbing and non-absorbing particles.

2.5 Fractional non-BC absorption from BrC

Many previous studies of BrC assume that BrC does not absorb significant amounts of light at long wavelengths (532–705 nm) (Wonaschütz et al., 2009; Lack et al., 2012a; Taylor et al., 2020; Zeng et al., 2021; Zhang et al., 2022). In this study, the PILS system was used to quantify the absorption of light for water-soluble BrC at 660 nm. This absorption is not likely caused by traditional BC, which is insoluble and will be removed by the PILS impactor and the 0.2 µm filter in PILS, and the BC over 110 nm in size will not be oxidized by the TOC analyzer (Peltier et al., 2007; Zeng et al., 2021; Sullivan et al., 2022).

To investigate which contributes more to absorption enhancement at 660 nm, the absorption from BrC or the lensing effect, the fractional non-BC absorption from BrC at 660 nm is calculated using Eq. (6):

$$\text{fractional } Abs_{BrC} = \frac{Abs_{BrC\_660}}{Abs_{Total\_660} - M_{BC} \cdot MAC_{BC\_core\_660}}, \quad (6)$$

where Abs_{Total_660} is the total absorption coefficient at 660 nm which is measured by the PAS, M_{BC} is the mass concentration of BC which is measured by the SP2, and $MAC_{BC\_core\_660}$ is the MAC of the BC core at 660 nm which

is set to 6.3 $m^2\ g^{-1}$ (Bond and Bergstrom, 2006; Subramanian et al., 2010). Abs_{BrC_660} is the total BrC absorption coefficient at 660 nm, which is calculated from the water-soluble light absorption provided by PILS, where we convert absorption from water-soluble BrC to total BrC. More specifically, to convert the measured light absorption by water-soluble organics into total BrC absorption in the ambient, it had to be multiplied by two factors. The first factor converts absorption from water-soluble BrC into absorption from total BrC. This factor is obtained by taking the ratio between OM and WSOM. Water-soluble organic mass is calculated from the PILS WSOC data using a WSOM : WSOC ratio of 1.6 (Duarte et al., 2015, 2019). Ambient organic mass is measured by AMS or calculated from the particle size distributions measured by the UHSAS assuming the particle mass all comes from organic material with a particle density of 1.4 g cm^{-3}. Both methods are used and compared in this paper. The second factor accounts for the fact that particles absorb more light than the same substance in the bulk liquid phase. Here we use Mie theory (Bohren and Huffman, 1983) to convert absorption from BrC in aqueous solution to absorption from BrC particles in the ambient (Liu et al., 2013; Zeng et al., 2020). The complex refractive index ($m = n + ik$) was put into a Mie code (implemented in Igor by Ernie Lewis based on Bohren and Huffman, 1983) to obtain the absorption efficiency (Q), and it was further used to calculate the absorption coefficient with Eq. (7) (Liu et al., 2013). The real part of the refractive index (n) is set to 1.55, and the imaginary part is calculated using Eq. (8) (Liu et al., 2013):

$$\mathrm{Abs}\left(\lambda, D_\mathrm{p}\right) = \frac{3}{2} \cdot \frac{Q \cdot \mathrm{WSOC}}{D_\mathrm{p} \cdot \rho}, \tag{7}$$

$$k = \frac{\rho\lambda \cdot \mathrm{H_2O\_Abs}(\lambda)}{4\pi \cdot \mathrm{WSOC}}, \tag{8}$$

where λ is the wavelength, D_p is the diameter of the particle, $\mathrm{Abs}(\lambda, D_\mathrm{p})$ is the absorption coefficient, Q is the absorption efficiency, the particle density (ρ) is set to 1.4 g cm^{-3}, WSOC is the mass concentration of WSOC (µg C m^{-3}) measured by PILS, and $H_2O\_Abs(\lambda)$ is the water-soluble light absorption coefficient measured by PILS. The plume-averaged particle size distribution was used in the calculation, and then the absorption coefficient was calculated for each size bin of UHSAS to obtain the most accurate Mie factor for each plume.

The average OM : WSOM factor based on the UHSAS (UHSAS factor) for all the plumes is 2.36 with a standard deviation of 1.17. The average OM : WSOM based on AMS (AMS factor) is 1.63 with a standard deviation of 0.74. The average Mie factor at 660 nm is 1.47 (standard deviation of 0.13), which is close to the factor of 1.36 found by Zeng et al. (2022) based on FIREX data. The Mie factor at 405 nm based on the WE-CAN data is also calculated, with an average of 1.83 that is similar to the factors that Zeng et al. (2022) determined at 405 nm (1.7) based on FIREX and that Liu et al. (2013) determined at 450 nm (1.9) based on measurements in Atlanta.

Sensitivity tests were done for these factors by choosing values from reasonable ranges for the particle density (1.1, 1.4, and 1.7 g cm^{-3}) and WSOM : WSOC ratio (1.5, 1.6, and 1.8) (Duarte et al., 2015, 2019; Finessi et al., 2012; Sun et al., 2011) (Table S1 in the Supplement). Particle density only affects the Mie factor and UHSAS factor, while the WSOM : WSOC ratio affects the AMS factor and UHSAS factor. As shown in Table S1, the impact of particle density on the Mie factor (at both 660 and 405 nm) is negligible, WSOM : WSOC being the only component that affects the AMS factor (ranging from 1.48 to 1.73), while the UHSAS factor is much more sensitive (ranging from 1.65 to 3.06) to both particle density and WSOM : WSOC. Overall, Table S1 demonstrates that none of the factors other than the UHSAS factor is sensitive to the exact parameters chosen for the calculation, giving confidence that the results presented are robust.

This approach assumes that water-insoluble BrC has the same refractive index as water-soluble BrC. This assumption would provide a lower estimate of the BrC contribution to the total absorption because Sullivan et al. (2022) found that 45 % of the BrC absorption at 405 nm in WE-CAN came from water-soluble species, and Zeng et al. (2022) found that insoluble BrC absorbs more at higher wavelengths than soluble BrC. Methanol-insoluble BrC chromophores caused 87 % of the light absorption at 664 nm.

2.6 Absorption of BrC and water-soluble BrC

The bulk absorption coefficient of water-soluble BrC at a specific wavelength ($Abs_{ws\_BrC\lambda}$) is measured directly by the PILS system. The bulk absorption coefficient of BrC is calculated from Eq. (9):

$$\mathrm{Abs_{BrC+lensing\_\lambda}} = \mathrm{Abs_{Total\_\lambda}} - M_\mathrm{BC} \cdot \mathrm{MAC_{BC\_core\_\lambda}}, \tag{9}$$

where Abs_{Total_λ} is the total absorption coefficient measured by the PAS. The MAC of the BC core is set to 6.3 and 10.2 $m^2\ g^{-1}$, respectively, at 660 and 405 nm. It should be noted that both BrC and lensing contribute to the bulk absorption coefficient and cannot be separated using this approach.

Then the plume-integrated absorption and scattering were normalized (x/CO) by taking the ratio of background-subtracted absorption or scattering (Δx) to the background-subtracted CO mixing ratio (ΔCO) (Eq. 10), so that the change in the normalized properties is not impacted by dilution of the plume with background air.

$$x/\mathrm{CO} = \frac{\Delta x}{\Delta \mathrm{CO}} \tag{10}$$

2.7 Modified combustion efficiency (MCE)

The variation of burn condition (e.g., flaming or smoldering) and fuel type can cause a significant difference in BC emissions and changes in aerosol properties (Akagi et al., 2011; Andreae, 2019). Burn conditions can be estimated with the MCE, defined as in Eq. (11):

$$\mathrm{MCE} = \frac{\Delta \mathrm{CO_2}}{\Delta \mathrm{CO} + \Delta \mathrm{CO_2}}, \quad (11)$$

where ΔCO_2 and ΔCO are the background-subtracted CO_2 and CO mixing ratio. The background of the CO_2 and CO mixing ratio is obtained via the same process as described in Sect. 2.3.

3 Results and discussion

3.1 Comparison of WE-CAN MAC_{BrC} with modeling studies

It is challenging for climate models to simulate absorption from BrC, especially because it is highly wavelength-dependent and may change with chemical age (Liu et al., 2020). Recently, the Saleh et al. (2014) parameterization was implemented in models in an attempt to better parameterize the imaginary part of the BrC refractive index (Wang et al., 2018; Carter et al., 2021). To test how accurately the Saleh parameterization matched WE-CAN data, the BC : OA ratios measured during WE-CAN were input into the Saleh parameterization, which provides an imaginary part for the refractive index of BrC ($k_{\mathrm{BrC},\lambda}$) as a function of the BC : OA ratio. The plume-integrated BC : OA ratio for each plume was used in the parameterization, which gave average k_{BrC} values of 0.025, 0.013, and 0.009, respectively, at 405, 550, and 660 nm. Mie theory (Bohren and Huffman, 1983) was then used to calculate the MAC for BrC. To do the Mie calculations, we assumed a real part of the refractive index of 1.7 for BrC (same as in Saleh et al., 2014), used volume mean diameters measured for each plume, and used an organic density of 1.4 g cm^{-3}. Figure 2 compares the observed $MAC_{\mathrm{BrC+lensing}}$ (Eq. 4) and $MAC_{\mathrm{ws\_BrC}}$ (Eq. 5) with the value calculated from the Saleh parameterization with inputs from WE-CAN. In both the observations and parameterization, the MAC_{BrC} decreases as the wavelength increases. However, the Saleh parameterization is always significantly larger than the observations. The MAC_{BrC} values from the Saleh parameterization, which does not include lensing effects, are factors of 3.4 and 2.8 larger than the observed $MAC_{\mathrm{BrC+lensing}}$ at 405 and 660 nm, respectively. The range of BC : OA ratios during WE-CAN (0.007–0.061) is on the very small end of the range (0.005–0.7) used in Saleh et al. (2014), and the parameterization failed to capture absorbing aerosol properties for this study. The discrepancy could also be partly because the data Saleh et al. (2014) used for their parameterization came from controlled laboratory burns and not wildfires or because emissions observed during WE-CAN have

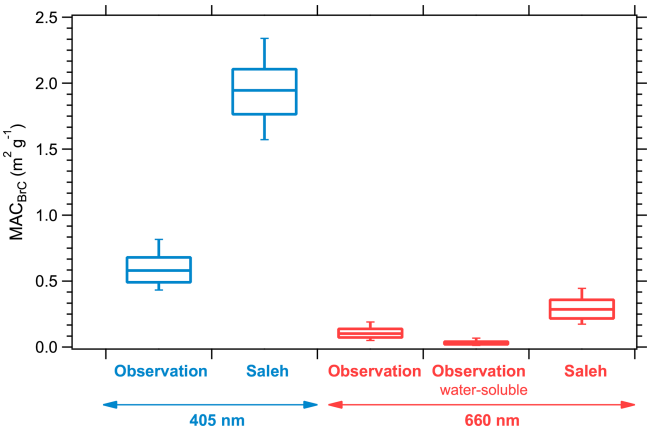

Figure 2. Boxplot summary for observed and parameterized (Saleh) MAC_{BrC} at 405 nm (blue) and 660 nm (red). For each box, the central line represents the median, the top and bottom edges represent the 75th and 25th percentiles, and the top and bottom whiskers represent the 90th and 10th percentiles of the data.

all undergone some near-source aging before being observed by the aircraft. It is worth noting that the Saleh parameterization of MAC_{BrC} is very sensitive to organic aerosol density. If particle density is increased from 1.4 to 1.7 g cm^{-3}, the Saleh parameterization's median MAC_{BrC} decreases to 1.6 and 0.24 m^2 g^{-1}, respectively, at 405 and 660 nm (factors of 2.8 and 2.3, respectively, compared to the observed MAC_{BrC} at 405 and 660 nm). The fact that the Saleh parameterization overestimates the absorption property of biomass aerosol, especially for freshly emitted aerosols, suggests that different parameterizations are needed for the western US. Carter et al. (2021) utilized the Saleh parameterization for BrC absorption in the GEOS-Chem model (a global model of atmospheric chemistry driven by meteorological input from the Goddard Earth Observing System) and also found that the Saleh model overestimated BrC absorption for WE-CAN. It was hypothesized that the overestimation was due to the lack of a bleaching process for BrC in the model and offset part of the overestimation by bringing bleaching into the model.

3.2 Investigation of BrC bleaching at visible wavelengths

A limited number of field measurements have shown BrC decay with chemical age (Forrister et al., 2015; Wang et al., 2016). Despite a relatively poor understanding of the mechanism of bleaching or whitening of BrC, this process has been implemented in numerous model simulations (Brown et al., 2018; Wang et al., 2018; Carter et al., 2021). While only a fraction of the organic aerosol mass absorbs light, both models and observations typically treat all organics as equally absorbing because of an inability to distinguish between absorbing and non-absorbing molecules. The definition of bleaching or whitening was unclear in the previous literature. Models tend to treat bleaching as a change in the re-

fractive index or a decrease in the MAC (Brown et al., 2018; Wang et al., 2018; Carter et al., 2021), while observations or laboratory experiments mostly link bleaching to the decrease in normalized total absorption (Forrister et al., 2015; Palm et al., 2020; Zeng et al., 2022). It is important to distinguish between these two, because the decrease in the absorption coefficient can also be caused by a loss of absorbing organic material, which will also change the scattering coefficient and radiative forcing. Therefore, the MAC of BrC and the absorption coefficient of BrC at visible wavelengths were calculated and analyzed together with two chemical clocks (O : C and toluene : benzene ratios) and organic mass to determine whether BrC bleached during the WE-CAN campaign and whether the bleaching was caused by the less organic mass or the change in the refractive index. Because all large wildfire emissions are a mix of different regions that burn slightly different fuels at different combustion efficiencies and because models treat regions, not individual fires, we identify relationships in this paper that hold true across all the flight data collected during WE-CAN. These types of broad correlations are much more useful than individual case studies yielding results that only hold true sometimes.

3.2.1 Consistency of the mass absorption cross section of BrC at 405 nm

Palm et al. (2020) combined data from WE-CAN and the Monoterpene and Oxygenated aromatic Oxidation at Night and under LIGHTs (MOONLIGHT) chamber experiment and found that evaporated biomass burning POA is the dominant source of biomass burning SOA in wildfire plumes during the first few hours after emission. They also found that, of the SOA formed from oxidation, phenolic compounds contribute 29 ± 15 % of the BrC absorption at 405 nm. In this section, we analyze the characteristics of BrC at 405 nm to understand the average properties of BrC and to understand the balance of BrC formation and bleaching during WE-CAN. The MAC of BrC is calculated using Eq. (4), and therefore it includes a contribution from the lensing effect. The MAC of water-soluble BrC is calculated using Eq. (5). Figure 3 shows the MAC of BrC at 405 nm and the aerosol oxidation level (O : C ratio), while Fig. S2 in the Supplement is a similar plot that uses a simple photochemical clock, the gas-phase toluene : benzene ratio. The O : C ratio characterizes the oxidation state of OA and typically increases with photochemical age (Aiken et al., 2008), while the toluene : benzene ratio decreases with photochemical processing time since toluene is more reactive than benzene (Gouw et al., 2005). Both markers are commonly used to indicate the chemical age of smoke, and they correlated well with each other during WE-CAN (Fig. S1 in the Supplement).

$MAC_{BrC+lensing\_405}$ varies from 0.08 to 1.6 $m^2\,g^{-1}$ with a mean value of 0.59 $m^2\,g^{-1}$ and a standard deviation of 0.19. The largest values are from RF05, the flight through California, Oregon, and Idaho, where aged smoke from different fires was mixed. The large $MAC_{BrC+lensing\_405}$ occurred when the aircraft left the smoke-filled boundary layer during RF05. If we exclude $MAC_{BrC+lensing\_405}$ from RF05, the values range from 0.08 to 1.09 $m^2\,g^{-1}$ but still have a mean value of 0.59 $m^2\,g^{-1}$ and a standard deviation of 0.15. Again, we note that this value includes the contribution of lensing. Despite this, our results lie in the same range as those measured without the contributions of lensing of 0.31 ± 0.09 $m^2\,g^{-1}$ measured in CLARIFY-2017 (Taylor et al., 2020), 0.13–2.0 $m^2\,g^{-1}$ measured in FIREX-AQ (Zeng et al., 2022), and 0.25–1.18 $m^2\,g^{-1}$ measured in ORACLES (Zhang et al., 2022). Very weak trends or non-trends are observed in the chemical markers of aging (Fig. 3). If there is any trend, it is a slight increase in MAC_{ws_BrC405}, with an O : C ratio with a poor correlation. A similar weak trend is also observed when comparing MAC_{ws_BrC405} and $MAC_{BrC+lensing\_405}$ with the toluene : benzene ratio (Fig. S2). The flat or slightly increasing trend with an increasing oxidation level and a decreasing toluene : benzene ratio suggests that the refractive index of BrC does not change in a consistent way at 405 nm. It is important to remember that most of the trends observed in WE-CAN are caused by emissions from different fires compared to variations within a single fire, which tend to be quite small. Only two flights show a clear trend ($R^2 > 0.3$) for both MAC_{ws_BrC405} and $MAC_{BrC+lensing\_405}$ with an increasing O : C ratio at the same time, and they are RF03 (R^2 values of 0.85 and 0.85 with positive slopes for MAC_{ws_BrC405} and $MAC_{BrC+lensing\_405}$) and RF06 (R^2 values of 0.8 and 0.49 with negative slopes for MAC_{ws_BrC405} and $MAC_{BrC+lensing\_405}$), where RF03 only measured a single fire (the Taylor Creek fire).

RF05 and RF08 were chosen as case studies to observe the optical properties of highly aged aerosol to see whether the optical properties of this aerosol were similar to those observed in the near-field plume sampling of individual fires at the highest chemical or physical age observed, which was roughly 6–24 h of physical aging. RF08 was a flight through the Central Valley of California, where aged smoke from

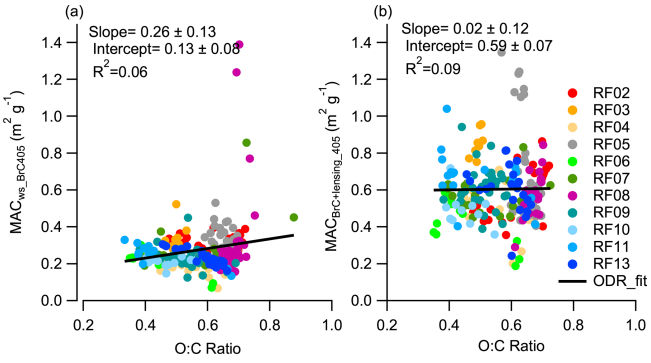

Figure 3. Plume-integrated **(a)** MAC_{ws_BrC405} and **(b)** $MAC_{BrC+lensing\_405}$ variations with the organic aerosol O : C ratio.

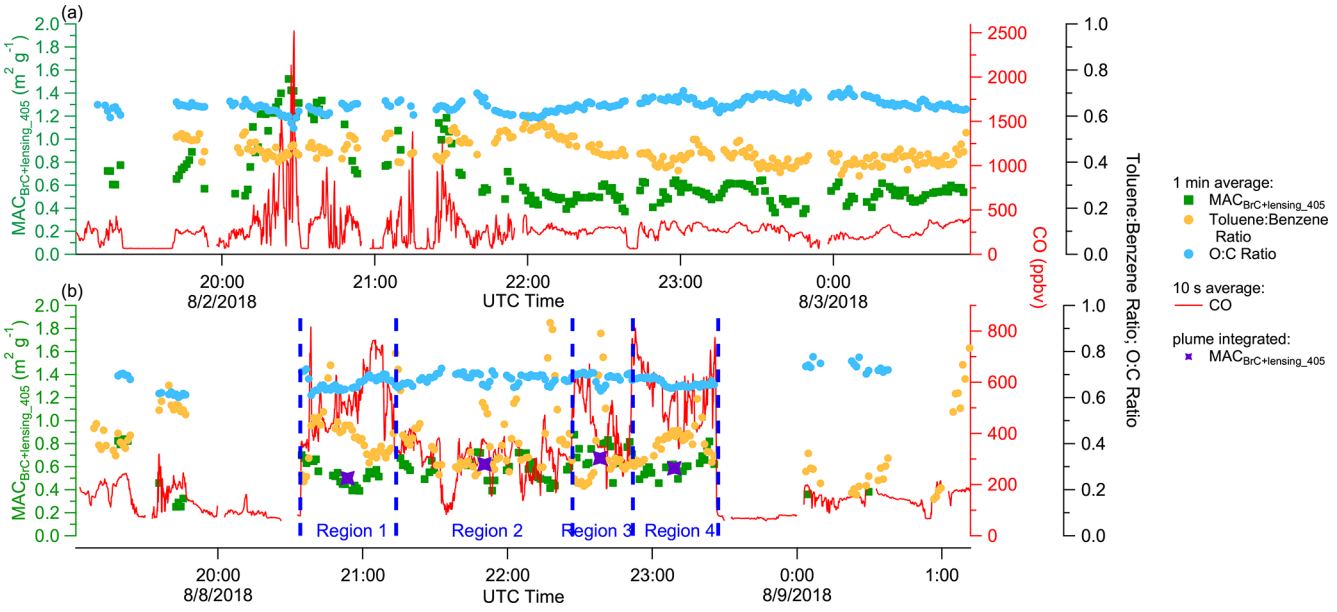

Figure 4. Time series of plume properties during **(a)** RF05 (measurements far from the fire source) and **(b)** RF08 (Central Valley of California). The different square and round markers indicate 1 min averages of different variables as shown in the legend, and the red solid line represents 10 s averages of the mixing ratio of CO. The purple stars in RF08 indicate region-integrated $MAC_{BrC+lensing\_405}$ (individual regions are separated based on the concentration of CO and are indicated by the blue dashed lines).

multiple fires that had settled in the valley was measured, while RF05 was a flight on which smoke from several California fires was observed in California, Oregon, and Idaho, roughly 450–1000 km from the fires (the flight paths are shown in Fig. 1). The $MAC_{BrC+lensing\_405}$, the CO mixing ratio, the toluene : benzene ratio, and the O : C ratio are displayed in Fig. 4a and b. The mixing ratio of CO is relatively low in these aged diluted smoke plumes compared to the plumes near the sources analyzed earlier; 1 min averages of $MAC_{BrC+lensing\_405}$ are calculated to reduce noise, and 1 min averages for the toluene : benzene ratio and the O : C ratio are calculated and all negative values removed. As shown in Fig. 4, the smallest toluene : benzene ratios are $\sim$0.35 in RF05 and $\sim$0.16 in RF08, while the largest O : C ratio is $\sim$0.7 in both RF05 and RF08, which indicates that these two cases indeed captured plumes that appear chemically aged to a similar extent to the other near-source flights, where the smallest toluene : benzene ratio was 0.33 and the largest O : C ratio was 0.88 in near-fire measurements (Figs. 3, S2, and S6a in the Supplement).

In RF05 (Fig. 4a), the weighted average O : C ratio over the entire flight was 0.64, and the toluene : benzene ratio averaged 0.45 with a standard deviation of 0.05. $MAC_{BrC+lensing\_405}$ varied from 0.36 to 1.52 $m^2\,g^{-1}$ with an average of 0.66 $m^2\,g^{-1}$ and a standard deviation of 0.26 $m^2\,g^{-1}$. The plume that was measured on this flight was a mixture of different fire sources. Despite the much longer transit time and distance, overall, these emissions, which were measured 450–1000 km away, have a very similar $MAC_{BrC+lensing\_405}$ to that of the near-source flights, where we tracked emissions from as near to the fire source as allowed by air traffic control.

The RF08 (Fig. 4b) results are similar to those of RF05, even though these emissions were smoke of mixed ages from multiple fire sources in the Central Valley of California. The weighted average O : C ratio was 0.67 over the entire measurement, and the average toluene : benzene ratio was 0.41 with a standard deviation of 0.15. The $MAC_{BrC+lensing\_405}$ average is 0.59 $m^2\,g^{-1}$ with a standard deviation of 0.14 $m^2\,g^{-1}$. There are several extreme values that exist in the dataset, probably because of the SP2 hysteresis caused by variation in the dilution rate of the SP2 that cannot be totally eliminated from the 1 min average. In addition, the smoke from RF08 (Fig. 4b) is split into four regions based on varying observed CO mixing ratios, and an integrated $MAC_{BrC+lensing\_405}$ is calculated for each region (purple star marker). The regional edges are represented by blue dashed lines. The integrated $MAC_{BrC+lensing\_405}$ for all of these variable CO regions is relatively stable, with an average of 0.59 $m^2\,g^{-1}$ and a standard deviation of 0.07 $m^2\,g^{-1}$.

3.2.2 Decrease in absorption at 405 nm observed with markers of chemical oxidation

Although neither $MAC_{BrC+lensing\_405}$ nor MAC_{ws_BrC405} decreases with O : C or toluene : benzene, Fig. 5 shows that BrC bleaching is observed in terms of decreased total absorption. Figure 5a and c show the behavior of BrC absorption at 405 nm with markers of the aerosol oxidation

level (O : C) and photochemistry (toluene : benzene). The absorption coefficient of BrC shown in Fig. 5 is calculated using Eqs. (9)–(10), which cannot separate the absorption caused by the BrC and lensing effect. To confirm that the observed trends are not a result of changing lensing, the absorption coefficient of water-soluble BrC measured by PILS, which does not include lensing effects, is also compared in Fig. 6a and c. The average water-soluble BrC absorption at 405 nm (Abs_{ws_BrC405}, 0.02 Mm^{-1} $ppbv^{-1}$) which is directly measured by PILS is only 20 % of the total absorption from BrC plus lensing ($Abs_{BrC+lensing\_405}$, 0.11 Mm^{-1} $ppbv^{-1}$), which is calculated from the PAS and SP2 (Eq. 9). However, $Abs_{BrC+lensing\_405}$ and Abs_{ws_BrC405} both decrease with increasing O : C ($R^2 = 0.65$ and $R^2 = 0.3$, respectively, for $Abs_{BrC+lensing\_405}$ and Abs_{ws_BrC405}) and decreasing toluene : benzene ratios, which suggests a similar level of decreasing BrC absorption for all the fires observed in WE-CAN from numerous locations in the western US. This relationship holds despite differences in the fuel types, burn conditions, and meteorologies of all of these fires. The observed trends are mostly due to the decrease in both total OA mass (Fig. 5b and d) and WSOC (Fig. 6b and d) with the increasing O : C ratio ($R^2 = 0.8$ and $R^2 = 0.4$, respectively, for OA and WSOC) and the decreasing toluene : benzene ratio ($R^2 = 0.64$ and $R^2 = 0.44$, respectively, for OA and WSOC). Overall, the organic aerosol O : C ratio predicts the BrC evolution better than the toluene : benzene ratio, probably because it is a particle-phase property rather than a gas-phase one. Again, it is important to clarify whether BrC bleaching is caused by a decreasing BrC absorption coefficient or a decreasing BrC refractive index (or MAC). In this study, a decreasing MAC_{BrC} is not observed. Rather, the BrC absorption coefficient decreases significantly with the simple O : C and toluene : benzene chemical clocks due to the loss of OA mass. Less OA mass also causes a decrease in the bulk scattering coefficient (Fig. S3 in the Supplement), leading to a very different net radiative effect than when reducing MAC_{BrC}.

It is important to recall that we aimed to find general trends that hold for all fires in the western US, and the above trend is significant when all fires are grouped together, although the trend is, in fact, not robust on each flight and is rather due to variations between the fire plumes than variations within a single fire plume. Figure 7 shows the correlation between the normalized OA and chemical age for each fire source. This demonstrates that different fires show different relationships and that OA does not always decrease with oxidation level or chemical aging within a single fire (Kiwah fire and Rabbitfoot fire), though an increasing O : C ratio does correlate well ($R^2 > 0.3$) with decreasing OA mass in seven fires (with R^2 values of 0.94 for the Taylor Creek fire, 0.87 for the Carr fire, 0.86 for the Beaver Creek fire, 0.8 for the Coal Hollow fire, 0.76 for the Bear Trap fire, 0.35 for the Sharps fire, and 0.31 for the Sugarloaf fire). The toluene : benzene ratio did not track OA as well as the O : C ratio, and a decreasing toluene : benzene ratio correlates well ($R^2 > 0.3$) with decreasing OA mass in three fires (with R^2 values of 0.87 for the Rabbitfoot fire, 0.85 for the Coal Hollow fire, and 0.84 for the Bear Trap fire).

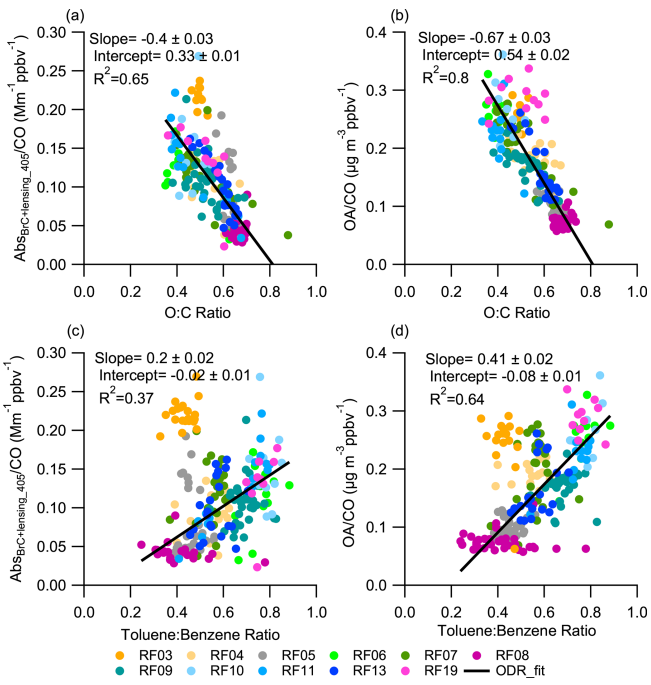

Figure 5. Plume-integrated normalized $Abs_{BrC+lensing\_405}$ and OA variation with chemical age. The top panels show the **(a)** plume-integrated normalized $Abs_{BrC+lensing\_405}$ and **(b)** plume-integrated normalized OA variation with the O : C ratio. The bottom panels show the **(c)** plume-integrated normalized $Abs_{BrC+lensing\_405}$ and **(d)** plume-integrated normalized OA variation with the toluene : benzene ratio. Data from RF03 were excluded from the ODR fit with the toluene : benzene ratio, because RF03 sampled the injection of fresh smoke into the free troposphere, where gas species reacted more rapidly than particles and the toluene : benzene ratio failed to keep track of the aerosol evolution.

No trend is observed in CO-normalized OA mass with plume physical age (Fig. S4 in the Supplement), which is consistent with the result from Garofalo et al. (2019) in that no net OA mass change was observed in individual plumes during WE-CAN when they are characterized by their physical age, although more data from additional fires were included in the current work. Plume-integrated CO-normalized OA also shows a weak trend or no trend with altitude and temperature (Fig. S5 in the Supplement). However, we note that the smallest OA : CO ratio was captured in the plumes (RF08) that have the highest temperature (∼ 305 K), and larger OA : CO ratios tend to be observed in colder plumes (RF19). More studies are needed to determine how much OA is evaporated in high-temperature plumes because the WE-CAN dataset does not capture enough temperature variation within plumes to draw a robust conclusion. No clear trend was found between $MAC_{BrC+lensing\_405}$ and physical

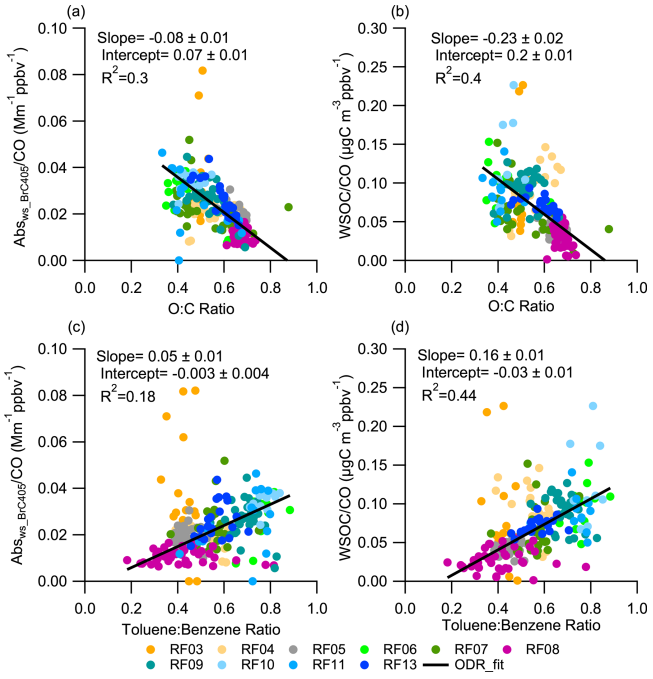

Figure 6. Similar to Fig. 5 but with the plume-integrated normalized Abs_{ws_BrC405} from PILS in panels **(a)** and **(c)** and WSOC in panels **(b)** and **(d)**.

age or MCE (Fig. S6). Similar behavior was also observed in western wildfires at 405 nm in FIREX-AQ (Zeng et al., 2022). Part of the reason for this is that, for most fires, we only captured the first few hours (< 15 h), and MCE does not have a robust capability to predict biomass burning particle properties (McClure et al., 2020). No trend is found between $MAC_{BrC+lensing\_405}$ and altitude or temperature (Fig. S7 in the Supplement). The trend in the BC : OA ratio (Fig. S8 in the Supplement) is not as clear as in Saleh et al. (2014), most probably because the range of BC : OA ratios observed during WE-CAN (0.007–0.061) is much smaller than that (0.005–0.7) observed in the work of Saleh et al. (2014). Even in their work, the increasing trend is not very clear if one only focuses on the region where the BC : OA ratio is less than 0.03. Also, the Saleh et al. (2014) results were obtained from laboratory burns and not from wildfires, which might also cause a discrepancy.

3.2.3 Mass absorption cross section and optical properties of BrC at 660 nm

BrC is defined as OA that has strong absorption at UV and shorter visible portions of the spectrum and historically has been considered to be almost transparent near the red wavelengths (Andreae and Gelencsér, 2006; Bahadur et al., 2012; Liu et al., 2020). However, during WE-CAN, we were able to quantify Abs_{ws_BrC660} with the PILS instrument. We know that absorption observed in PILS at 660 nm is not BC because BC is insoluble and will be removed by the PILS impactor, the 0.2 µm filter in the instrument, and that BC over 110 nm in size will not be oxidized by the TOC analyzer (Peltier et al., 2007; Zeng et al., 2021; Sullivan et al., 2022). Next, we investigate the behavior of BrC absorption at 660 nm to see whether BrC has similar behavior at the long and short ends of the visible spectrum.

Figure 8 shows the behavior of brown carbon at 660 nm compared to the O : C ratio. Similar to 405 nm, no bleaching in terms of decreased MAC is observed at 660 nm. If there is any trend, it is increasing MAC_{ws_BrC660} and $MAC_{BrC+lensing\_660}$ with the organic aerosol O : C ratio. Similar trends are observed, though with lower correlation, in the toluene : benzene ratio (Fig. S9 in the Supplement). The mean value of $MAC_{BrC+lensing\_660}$ is 0.11 $m^2\ g^{-1}$ (with a standard deviation of 0.06), which is much larger than the 0.03 average of MAC_{ws_BrC660}, a result we have attributed to the lensing effect but which could also partially be a result of water-insoluble BrC having a higher MAC than water-soluble BrC.

These results for the behavior of MAC_{BrC} at different wavelengths derived using different instruments (PAS and PILS) are further evidence that MAC_{BrC} does not decrease with physical or chemical age in the WE-CAN dataset. At a minimum, the plume-integrated results, which represent the total optical properties relevant to climate models, do not capture any MAC_{BrC} decay that might be occurring at the edges of the plume.

Similarly to our analysis at 405 nm, RF05 and RF08 are presented as case studies to investigate the behavior of $MAC_{BrC+lensing\_660}$ in aged plumes emitted from different fire sources. Figure 9 is similar to Fig. 4, but with $MAC_{BrC+lensing\_660}$ instead of $MAC_{BrC+lensing\_405}$. For the case of RF05 (Fig. 9a), $MAC_{BrC+lensing\_660}$ varied from 0.04 to 0.40 $m^2\ g^{-1}$ with an average of 0.15 $m^2\ g^{-1}$ and a standard deviation of 0.07 $m^2\ g^{-1}$. $MAC_{BrC+lensing\_660}$ tends to be larger when the CO mixing ratio is higher but does not have a significant correlation with any marker of oxidation level or photochemistry shown in Fig. 9. For the case of RF08 (Fig. 9b), $MAC_{BrC+lensing\_660}$ is more stable than in RF05 and varied from 0.04 to 0.37 $m^2\ g^{-1}$ with an average of 0.18 $m^2\ g^{-1}$ and a standard deviation of 0.06 $m^2\ g^{-1}$. The region-integrated $MAC_{BrC+lensing\_660}$ is even more stable, with an average of 0.16 $m^2\ g^{-1}$ and a standard deviation of 0.01 $m^2\ g^{-1}$. Similar to the results at 405 nm, we observe that the MAC in these very aged plumes is very similar to the average MAC observed in the near field.

The normalized $Abs_{BrC+lensing\_660}$ and total scattering coefficient at 660 nm (Fig. S10 in the Supplement), together with the normalized Abs_{ws_BrC660} (Fig. S11 in the Supplement), were also investigated to see whether they decreased with markers of chemical age similar to the results seen at 405 nm. However, the correlation between these BrC optical properties and the O : C ratio or toluene : benzene ratio at 660 nm is much weaker and flat-

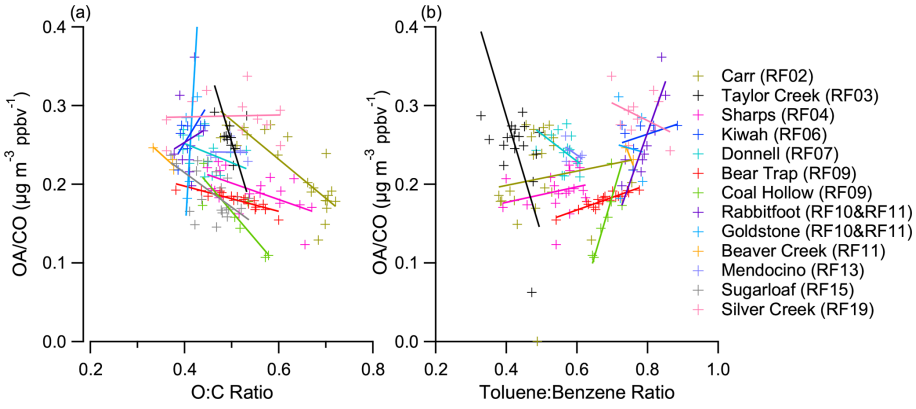

Figure 7. Plume-integrated normalized OA variation with the **(a)** O : C ratio and **(b)** toluene : benzene ratio. Different colors were used to distinguish plumes from different fire sources. Plumes from uncertain fire sources (especially plumes from RF05 and RF08) were not included in this plot.

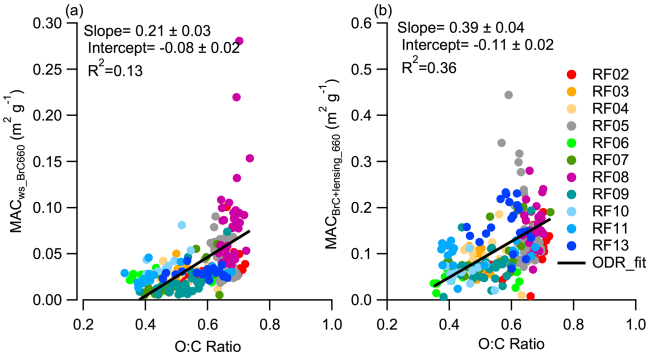

Figure 8. Plume-integrated **(a)** MAC_{ws_BrC660} and **(b)** $MAC_{BrC+lensing\_660}$ variations with the O : C ratio.

ter than at 405 nm. Perhaps this is because BrC absorption is very low at 660 nm, and high uncertainty is introduced by the assumptions required for calculation of this property and the instrumental uncertainties. The average normalized $Abs_{BrC+lensing\_660}$ is 0.02 Mm^{-1} $ppbv^{-1}$, which is 5 times lower than the absorption at 405 nm, while the average normalized Abs_{ws_BrC660} is 1 order of magnitude lower than Abs_{ws_BrC405}. The $MAC_{BrC+lensing\_660}$ (Fig. S12 in the Supplement) shows better correlation with the BC : OA ratio than $MAC_{BrC+lensing\_405}$, though the increasing trend is still not as significant as in Saleh et al. (2014) due to a much smaller BC : OA ratio during WE-CAN.

3.3 Relative importance of BrC and the lensing effect at 660 nm

Plume-integrated MAC_{BC} values at 660 nm (MAC_{BC660}) from the 13 WE-CAN research flights with clear plume transects of biomass burning plumes are shown in Fig. 10. The MAC_{BC660} discussed in this section is calculated using Eq. (3) and has contributions from absorption from the BC core, the BrC shell, and the lensing effect. Again, even fire plumes from individually named fires are usually a mix of many different burning conditions, and it is hard to identify the exact source in most wildfire smoke measurements, especially for well-mixed plumes. Therefore, flight-to-flight data are analyzed because each flight covered a region, and overall behavior of absorbing aerosol from wildfires can be provided. MAC_{BC660} varies between different flights, with RF03 having the highest average MAC_{BC660} of 12.9 m^2 g^{-1} and RF10 having the lowest average MAC_{BC660} of 8.6 m^2 g^{-1}. Even in highly aged plumes with emissions mixed from multiple fires (RF05 and RF08), MAC_{BC660} is similar in magnitude and consistency, with an average of 11.3 ± 1.8 m^2 g^{-1}. The average of all the plume-integrated MAC_{BC660} values is 10.9 m^2 g^{-1}, with a standard deviation of 2.1 m^2 g^{-1}. This result is similar to some other recent airborne measurements. Subramanian et al. (2010) reported a MAC_{BC660} of 10.9 ± 2.1 m^2 g^{-1} using an SP2 and PSAP operated during the MILAGRO campaign, which included airborne measurements of biomass burning over Mexico. Similarly, Zhang et al. (2017) estimated a MAC_{BC660} of 10 m^2 g^{-1} utilizing an SP2 and PSAP deployed on the NASA DC-8 research aircraft for the DC3 campaign, which measured the upper-tropospheric BC over the central US. Taylor et al. (2020) calculated a MAC_{BC655} of 12 ± 2 $m^2 g^{-1}$ for biomass burning emissions from Africa over the southeastern Atlantic Ocean, using airborne measurements from an SP2 and PAS during the CLARIFY-2017 campaign.

These results are encouragingly similar given the breadth of measurement techniques (PSAP is filter-based, whereas PAS is a direct measurement), geographic regions (continental US for DC3, Mexico for MILAGRO, African outflow for CLARIFY), and altitudes in the atmosphere (all were airborne campaigns covering a range of altitudes). If we apply 6.3 m^2 g^{-1} as the MAC of a BC core at 660 nm (Bond and Bergstrom, 2006; Subramanian et al., 2010), then the average absorption enhancement for the entire WE-CAN cam-

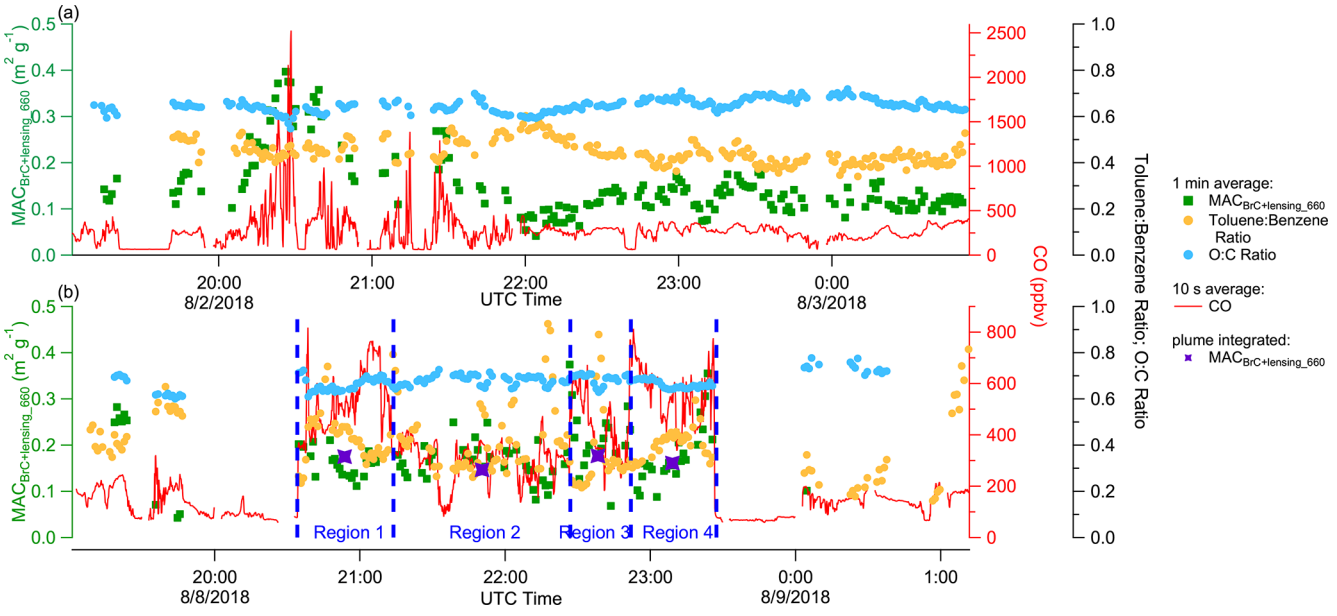

Figure 9. Time series of plume properties during **(a)** RF05 and **(b)** RF08 (Central Valley of California). The different square and round markers indicate 1 min averages of the different variables as shown in the legend, and the red solid line represents 10 s averages of the mixing ratio of CO. The purple stars in RF08 indicate the region-integrated $MAC_{BrC+lensing\_660}$ (individual regions are separated based on the concentration of CO and are indicated by the blue dashed lines).

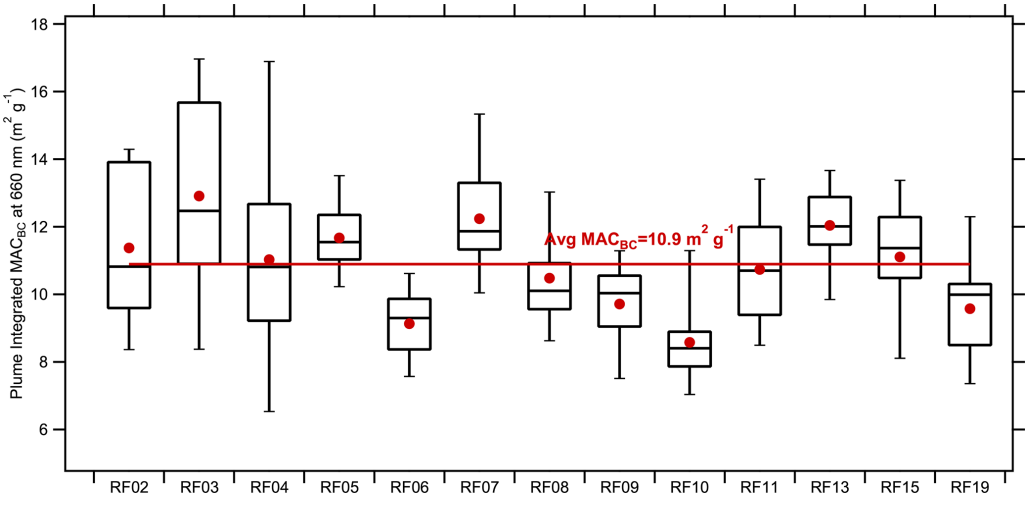

Figure 10. Boxplots of the plume-integrated MAC_{BC660} for each flight. In each box the central line represents the median, the top and bottom edges represent the 75th and 25th percentiles, and the top and bottom whiskers represent the 90th and 10th percentiles of the data. The red dot shows the average, and the red line indicates the average value for all plume-integrated MAC_{BC660}.

paign is 1.7. This means that the absorption of coated BC is 1.7 times higher than bare BC at 660 nm, which is somewhat close to the factor of ~ 2 reported by laboratory experiments (Schnaiter et al., 2005; Peng et al., 2016), larger than some field measurements (Cappa et al., 2012, 2019; Healy et al., 2015), and close to the 1.85 ± 0.45 measured by Taylor et al. (2020) in African biomass burning plumes. The similarity to the Taylor et al. (2020) result suggests global similarities in the MAC_{BC660} from aerosol emitted from wildfires.

MAC_{BC660} is also compared with the physical age and MCE (Fig. S13 in the Supplement), the O : C and toluene : benzene chemical clocks (Fig. S14 in the Supplement), the altitude, the temperature, and the dilution (ΔCO) (Fig. S15 in the Supplement). However, no clear trend is found in these comparisons.

The average absorption enhancement of 1.7 at 660 nm in this study indicates that, on average, 41 % of the total absorption at 660 nm is caused by lensing and absorbing organics

instead of BC itself. Figure 11 shows the fraction of non-BC absorption from BrC at 660 nm for the biomass burning plumes encountered during WE-CAN using Eqs. (6)–(8) with OM calculated from AMS. The figure is plotted against plume physical age to allow visualization of the variability, though there is no clear trend with physical age other than perhaps a decrease in variability with increasing physical age. Figure S16 in the Supplement shows a similar result when using OM calculated from the UHSAS. More details on the calculation and the AMS and UHSAS methods are given in Sect. 2.5. Assuming a MAC of the BC core of 6.3 $m^2\ g^{-1}$, BrC contributes roughly the same amount of absorption at 660 nm as lensing (46 % from the AMS method, 62 % from the UHSAS method). This means that 19 % (AMS method) to 26 % (UHSAS method) of the total absorption at 660 nm comes from BrC. When different particle density and WSOM : WSOC ratios are considered (top and bottom whiskers, red and blue dashed lines), the fractions of non-BC absorption are 41 %–49 % for the AMS approach (Fig. 11) and 43 %–80 % for the UHSAS approach (Fig. S16) based on different OM : OC ratios and densities. The UHSAS approach shows higher uncertainty because it is sensitive to the particle density when calculating the particulate mass (Table S1). While there is considerable variability between flights, a rule of thumb that roughly half of the non-BC absorption at the red wavelengths is from absorbing organic material seems reasonable. To the best of our knowledge, this is the first observation-based attempt to differentiate between lensing and absorbing organics at the red wavelengths. This approach assumes that water-insoluble BrC has the same refractive index as water-soluble BrC.

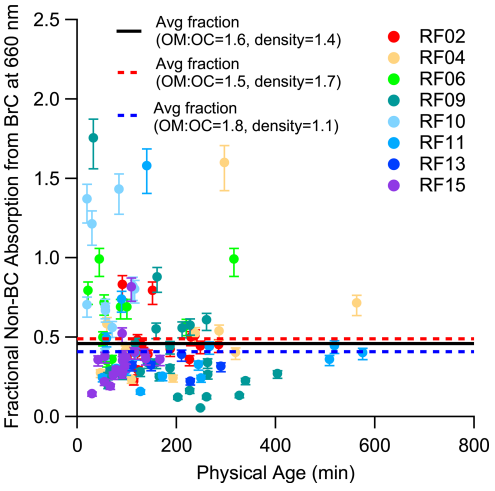

Figure 11. Time evolution of the fraction of non-BC absorption from BrC at 660 nm with AMS and the Mie factor. Markers were calculated using a density of 1.4 g cm^{-3} and a WSOM : WSOC ratio of 1.6. The top whiskers represent sensitivity test values using a density of 1.7 g cm^{-3} and a WSOM : WSOC ratio of 1.5, while the bottom whiskers represent sensitivity test values using a density of 1.1 g cm^{-3} and a WSOM : WSOC ratio of 1.8. The averaged fractions of non-BC absorption from BrC from all the plumes are shown with the black solid lines, while the ranges of this result from the sensitivity tests are shown with the red and blue dashed lines.

4 Conclusion

In this study, we presented results that enable a better understanding of the ability of aerosol emissions from wildfires to absorb visible light and how these properties change after emission. We presented mass absorption cross sections (MACs) for BC and BrC from western US wildfires measured during the WE-CAN campaign at both short and long visible wavelengths (MAC_{BC660}, $MAC_{BrC+lensing\_660}$, MAC_{ws_BrC660}, and $MAC_{BrC+lensing\_405}$). We also investigated the bulk absorption coefficient for BrC and the bulk scattering coefficient for total aerosol at both short and long visible wavelengths. General trends that held for all the fire sources were derived, which should be valid throughout the western US given the wide variety of emissions used to develop them.

By utilizing a common parameterization for the BrC refractive index from Saleh et al. (2014), with measured inputs for the BC : OA ratio and particle size, we calculated the theoretical MAC_{BrC660} and MAC_{BrC405}, and they were 2.3–3.4 times larger than the measured $MAC_{BrC+lensing}$ during WE-CAN. While this discrepancy has been resolved previously by implementing bleaching in model schemes, we showed that this is probably the incorrect explanation given that the MAC of BrC either remains constant or slightly increases when chemical markers (O : C, toluene : benzene) suggest that more oxidation has occurred. We suggest that a different parameterization of the refractive index is needed to represent wildfire optical properties in the western US rather than using bleaching to decrease the MAC of the Saleh parameterization. We also note that there needs to be better terminology to distinguish between decreasing absorption caused by losses of organic aerosol mass and decreasing absorption caused by changes in the MAC of the aerosol.

At the blue visible wavelengths, where BrC is more often thought about, $MAC_{BrC+lensing\_405}$ is $0.59 \pm 0.19\ m^2\ g^{-1}$ and shows little variation with physical age, MCE, altitude, temperature, or BC : OA ratio. There are no decreasing trends in the MAC_{BrC} data we obtained (MAC_{ws_BrC405}, $MAC_{BrC+lensing\_405}$, MAC_{ws_BrC660}, and $MAC_{BrC+lensing\_660}$) with markers of chemical age (toluene : benzene, O : C), but bulk absorption of BrC does decrease with these same markers. In highly aged plumes from multiple fires (RF05 and RF08), $MAC_{BrC+lensing\_405}$ has an average value of $0.63 \pm 0.2\ m^2\ g^{-1}$, suggesting that BrC remains significantly absorbing even at relatively higher ages.

We find that total organic aerosol (OA) and water-soluble organic carbon (WSOC) are strongly correlated with chemical markers of oxidative age. OA and WSOC (both normal-

ized to CO) decrease with a decreasing toluene : benzene ratio and an increasing O : C ratio. However, this phenomenon is only clearly observed when data from all the observed fires are included rather than during the aging of individual fire plumes. This could mean that the fires either had different emission ratios of toluene : benzene and O : C or that the smoke underwent rapid secondary chemistry prior to the first plume pass in WE-CAN. Regardless, the correlations are fairly robust (R^2 of 0.4 to 0.8) given the many variables (MCE, fuel type, etc.) that are changing in the dataset and provide a potential link between chemical markers and total organic aerosol amounts across a wide range of fires. OA and WSOC decreases with decreasing toluene : benzene or increasing O : C, MAC_{BrC} actually show a weak increasing trend with these same markers of aging, showing that, while the total amount of organic aerosol is decreasing, the ability of the organic aerosol to absorb by mass stays relatively constant or even increases. We also found that the bulk scattering coefficient (normalized to CO) decreases with a decreasing toluene : benzene ratio or an increasing O : C ratio due to less OA being present, which leads to a very different net radiative effect than that which results from just changing the refractive index of BrC.

At the red visible wavelengths, where BrC is often less noticed, we observed that the MAC of BC stayed relatively constant across all the plumes measured and at all physical ages (ages up to 15 h observed), with an averaged MAC_{BC660} of $10.9 \pm 2.1\,m^2\,g^{-1}$ (average $\pm$ standard deviation), which includes the contribution from both the lensing effect and absorbing organics. This average showed no clear trends with altitude or temperature, and we saw no evidence that MAC_{BC660} is correlated with MCE. Even in highly aged plumes with emissions mixed from multiple fires (RF05 and RF08), MAC_{BC660} is similar in magnitude to near-source plumes, with an average of $11.3 \pm 1.8\,m^2\,g^{-1}$. Both the fact that this MAC is significantly larger than the MAC for uncoated BC (often cited as $\sim 6.3\,m^2\,g^{-1}$) and the fact that the MAC remains relatively constant across different fires and different plume ages are key insights that can improve models of aerosol optical properties in wildfire emissions.

Through a novel use of PILS data, we find that BrC contributes 41 %–80 % of non-BC absorption at 660 nm (assuming $6.3\,m^2\,g^{-1}$ to be the MAC of the BC core at 660 nm). BrC contributes, on average, 26 % of the total absorption, but the absorption cross section of water-soluble BrC is relatively small at 660 nm, with a MAC_{ws_BrC660} of $0.03 \pm 0.02\,m^2\,g^{-1}$ that does not change with physical age, and no trend with MCE is observed. The average $MAC_{BrC+lensing\_660}$ derived from the PAS (which includes both brown carbon absorption and lensing of black carbon) is $0.11 \pm 0.06\,m^2\,g^{-1}$.

Data availability. The WE-CAN data can be found at https://data.eol.ucar.edu/master_lists/generated/we-can.

The DOIs for all the datasets used in this work are the following:

- PAS and CAPS PM_{SSA} at https://doi.org/10.26023/K8P0-X4T3-TN06 (Murphy, 2019);
- PILS1 at https://doi.org/10.26023/9H07-MD9K-430D (Sullivan, 2019) and https://doi.org/10.26023/CRHY-NDT9-C30V (Sullivan, 2021a);
- PILS2 at https://doi.org/10.26023/7TAN-TZMD-680Y (Sullivan, 2021b);
- SP2 at https://doi.org/10.26023/P8R2-RAB6-N814 (Levin, 2019);
- UHSAS at https://doi.org/10.26023/BZ4F-EAC4-290W (Toohey, 2019);
- PTR-ToF-MS at https://doi.org/10.26023/K9F4-2CNH-EQ0W (Hu and Permar, 2020);
- HR-AMS at https://doi.org/10.26023/MM2Y-ZGFQ-RB0B (Farmer and Kreidenweis, 2019);
- Picarro at https://doi.org/10.26023/NNYM-Z18J-PX0Q (Campos, 2019a); and
- miniQCL at https://doi.org/10.26023/Q888-WZRD-B70F (Campos, 2019b).

Supplement. The supplement related to this article is available online at: https://doi.org/10.5194/acp-24-12881-2024-supplement.

Author contributions. SMM designed the project. YS wrote the paper. YS, RPP, APS, EJTL, LAG, DKF, WP, LH, DWT, TC, EVF, and SMM collected and analyzed the data.

Competing interests. The contact author has declared that none of the authors has any competing interests.

Disclaimer. Publisher's note: Copernicus Publications remains neutral with regard to jurisdictional claims made in the text, published maps, institutional affiliations, or any other geographical representation in this paper. While Copernicus Publications makes every effort to include appropriate place names, the final responsibility lies with the authors.

Acknowledgements. The 2018 WE-CAN field campaign was supported by the US National Science Foundation through grant nos. AGS-1650493 (University of Wyoming), AGS-1650786 (Colorado State University), AGS-1650275 (University of Montana), and AGS-1650288 (University of Colorado at Boulder) and by the National Oceanic and Atmospheric Administration (award no. NA17OAR4310010, Colorado State University). This material is based upon studies supported by the National Center for Atmospheric Research, which is a major facility sponsored by the National Science Foundation under cooperative agreement no. 1852977. The authors acknowledge support through grant nos. AGS-1650493 for Yingjie Shen, Shane M. Murphy, and Rudra P. Pokhrel; AGS-1650786 for Amy P. Sullivan and Ezra J. T. Levin; AGS-1650275 for Lu Hu and Wade Permar; and AGS-1650288

for Darin W. Toohey. The NOAA Climate Program Office's Atmospheric Chemistry, Carbon Cycle, and Climate program (grant no. NA17OAR4310010) supported Delphine K. Farmer and Lauren A. Garofalo.

We sincerely thank Ernie Lewis for his work in implementing Mie theory in the Igor code.

Financial support. This research has been supported by the National Science Foundation (grant nos. AGS-1650493, AGS-1650786, AGS-1650275, AGS-1650288, and 1852977) and by the National Oceanic and Atmospheric Administration (grant no. NA17OAR4310010).

Review statement. This paper was edited by Dara Salcedo and reviewed by two anonymous referees.

References

Aiken, A. C., Decarlo, P. F., Kroll, J. H., Worsnop, D. R., Huffman, J. A., Docherty, K. S., Ulbrich, I. M., Mohr, C., Kimmel, J. R., Sueper, D., Sun, Y., Zhang, Q., Trimborn, A., Northway, M., Ziemann, P. J., Canagaratna, M. R., Onasch, T. B., Alfarra, M. R., Prevot, A. S. H., Dommen, J., Duplissy, J., Metzger, A., Baltensperger, U., and Jimenez, J. L.: O / C and OM / OC ratios of primary, secondary, and ambient organic aerosols with high-resolution time-of-flight aerosol mass spectrometry, Environ. Sci. Technol., 42, 4478–4485, https://doi.org/10.1021/es703009q, 2008.

Akagi, S. K., Yokelson, R. J., Wiedinmyer, C., Alvarado, M. J., Reid, J. S., Karl, T., Crounse, J. D., and Wennberg, P. O.: Emission factors for open and domestic biomass burning for use in atmospheric models, Atmos. Chem. Phys., 11, 4039–4072, https://doi.org/10.5194/acp-11-4039-2011, 2011.

Andreae, M. O.: Emission of trace gases and aerosols from biomass burning – an updated assessment, Atmos. Chem. Phys., 19, 8523–8546, https://doi.org/10.5194/acp-19-8523-2019, 2019.

Andreae, M. O. and Gelencsér, A.: Black carbon or brown carbon? The nature of light-absorbing carbonaceous aerosols, Atmos. Chem. Phys., 6, 3131–3148, https://doi.org/10.5194/acp-6-3131-2006, 2006.

Bahadur, R., Praveen, P. S., Xu, Y., and Ramanathan, V.: Solar absorption by elemental and brown carbon determined from spectral observations, P. Natl. Acad. Sci. USA, 109, 17366–17371, https://doi.org/10.1073/pnas.1205910109, 2012.

Bohren, C. F. and Huffman, D. R.: Absorption and scattering of light by small particless, John Wiley & Sons, New York, NY, USA, ISBN-10 0-471-29340-7, 1983.

Bond, T. C. and Bergstrom, R. W.: Light absorption by carbonaceous particles: An investigative review, Aerosol Sci. Tech., 40, 27–67, https://doi.org/10.1080/02786820500421521, 2006.

Bond, T. C., Habib, G., and Bergstrom, R. W.: Limitations in the enhancement of visible light absorption due to mixing state, J. Geophys. Res.-Atmos., 111, 1–13, https://doi.org/10.1029/2006JD007315, 2006.

Bond, T. C., Doherty, S. J., Fahey, D. W., Forster, P. M., Berntsen, T., Deangelo, B. J., Flanner, M. G., Ghan, S., Kärcher, B., Koch, D., Kinne, S., Kondo, Y., Quinn, P. K., Sarofim, M. C., Schultz, M. G., Schulz, M., Venkataraman, C., Zhang, H., Zhang, S., Bellouin, N., Guttikunda, S. K., Hopke, P. K., Jacobson, M. Z., Kaiser, J. W., Klimont, Z., Lohmann, U., Schwarz, J. P., Shindell, D., Storelvmo, T., Warren, S. G., and Zender, C. S.: Bounding the role of black carbon in the climate system: A scientific assessment, J. Geophys. Res.-Atmos., 118, 5380–5552, https://doi.org/10.1002/jgrd.50171, 2013.

Brown, H., Liu, X., Feng, Y., Jiang, Y., Wu, M., Lu, Z., Wu, C., Murphy, S., and Pokhrel, R.: Radiative effect and climate impacts of brown carbon with the Community Atmosphere Model (CAM5), Atmos. Chem. Phys., 18, 17745–17768, https://doi.org/10.5194/acp-18-17745-2018, 2018.

Brown, H., Liu, X., Pokhrel, R., Murphy, S., Lu, Z., Saleh, R., Mielonen, T., Kokkola, H., Bergman, T., Myhre, G., Skeie, R. B., Watson-Paris, D., Stier, P., Johnson, B., Bellouin, N., Schulz, M., Vakkari, V., Beukes, J. P., van Zyl, P. G., Liu, S., and Chand, D.: Biomass burning aerosols in most climate models are too absorbing, Nat. Commun., 12, 1–15, https://doi.org/10.1038/s41467-020-20482-9, 2021.

Burke, M., Driscoll, A., Heft-Neal, S., Xue, J., Burney, J., and Wara, M.: The changing risk and burden of wildfire in the United States, P. Natl. Acad. Sci. USA, 118, 1–6, https://doi.org/10.1073/PNAS.2011048118, 2021.

Campos, T.: Picarro G2401-m WS-CRDS CO2, CH4, CO and H2O in situ mixing ratio observations – ICARTT format, Version 1.2, UCAR/NCAR – Earth Observing Laboratory [data set], https://doi.org/10.26023/NNYM-Z18J-PX0Q, 2019a.

Campos, T.: Aerodyne CS-108 miniQCL CO, N2O and H2O in situ mixing ratio observations – ICARTT format, Version 1.2, UCAR/NCAR – Earth Observing Laboratory [data set], https://doi.org/10.26023/Q888-WZRD-B70F, 2019b.

Canagaratna, M. R., Jimenez, J. L., Kroll, J. H., Chen, Q., Kessler, S. H., Massoli, P., Hildebrandt Ruiz, L., Fortner, E., Williams, L. R., Wilson, K. R., Surratt, J. D., Donahue, N. M., Jayne, J. T., and Worsnop, D. R.: Elemental ratio measurements of organic compounds using aerosol mass spectrometry: characterization, improved calibration, and implications, Atmos. Chem. Phys., 15, 253–272, https://doi.org/10.5194/acp-15-253-2015, 2015.

Cappa, C. D., Onasch, T. B., Massoli, P., Worsnop, D. R., Bates, T. S., Cross, E. S., Davidovits, P., Hakala, J., Hayden, K. L., Jobson, B. T., Kolesar, K. R., Lack, D. A., Lerner, B. M., Li, S. M., Mellon, D., Nuaaman, I., Olfert, J. S., Petäjä, T., Quinn, P. K., Song, C., Subramanian, R., Williams, E. J., and Zaveri, R. A.: Radiative absorption enhancements due to the mixing state of atmospheric black carbon, Science, 337, 1078–1081, https://doi.org/10.1126/science.1223447, 2012.

Cappa, C. D., Zhang, X., Russell, L. M., Collier, S., Lee, A. K. Y., Chen, C. L., Betha, R., Chen, S., Liu, J., Price, D. J., Sanchez, K. J., McMeeking, G. R., Williams, L. R., Onasch, T. B., Worsnop, D. R., Abbatt, J., and Zhang, Q.: Light Absorption by Ambient Black and Brown Carbon and its Dependence on Black Carbon Coating State for Two California, USA, Cities in Winter and Summer, J. Geophys. Res.-Atmos., 124, 1550–1577, https://doi.org/10.1029/2018JD029501, 2019.

Carter, T. S., Heald, C. L., Cappa, C. D., Kroll, J. H., Campos, T. L., Coe, H., Cotterell, M. I., Davies, N. W., Farmer, D. K., Fox, C., Garofalo, L. A., Hu, L., Langridge, J. M., Levin, E. J. T., Murphy, S., Pokhrel, R., Shen, Y., Szpek, K., Taylor, J. W., and

Wu, H.: Investigating Carbonaceous Aerosol and its Absorption Properties from Fires in the western US (WE-CAN) and southern Africa (ORACLES and CLARIFY), J. Geophys. Res.-Atmos., 126, 1–28, https://doi.org/10.1029/2021JD034984, 2021.

Cho, C., Kim, S. W., Lee, M., Lim, S., Fang, W., Gustafsson, Ö., Andersson, A., Park, R. J., and Sheridan, P. J.: Observation-based estimates of the mass absorption cross-section of black and brown carbon and their contribution to aerosol light absorption in East Asia, Atmos. Environ., 212, 65–74, https://doi.org/10.1016/j.atmosenv.2019.05.024, 2019.

Craig, L., Moharreri, A., Schanot, A., Rogers, D. C., Dhaniyala, S., Craig, L., Anderson, B., and Dhaniyala, S.: Characterizations of Cloud Droplet Shatter Artifacts in Two Airborne Aerosol Inlets, Aerosol Sci. Tech., 47, 662–671, https://doi.org/10.1080/02786826.2013.780648, 2013a.

Craig, L., Schanot, A., Moharreri, A., Rogers, D. C., and Dhaniyala, S.: Design and Sampling Characteristics of a New Airborne Aerosol Inlet for Aerosol Measurements in Clouds, J. Atmos. Ocean. Tech., 30, 1123–1135, https://doi.org/10.1175/JTECH-D-12-00168.1, 2013b.

Craig, L., Moharreri, A., Rogers, D. C., Anderson, B., and Dhaniyala, S.: Aircraft-based aerosol sampling in clouds: Performance characterization of flow-restriction aerosol inlets, J. Atmos. Ocean. Tech., 31, 2512–2521, https://doi.org/10.1175/JTECH-D-14-00022.1, 2014.

Duarte, R. M. B. O., Freire, S. M. S. C., and Duarte, A. C.: Investigating the water-soluble organic functionality of urban aerosols using two-dimensional correlation of solid-state 13C NMR and FTIR spectral data, Atmos. Environ., 116, 245–252, https://doi.org/10.1016/j.atmosenv.2015.06.043, 2015.

Duarte, R. M. B. O., Piñeiro-Iglesias, M., López-Mahía, P., Muniategui-Lorenzo, S., Moreda-Piñeiro, J., Silva, A. M. S., and Duarte, A. C.: Comparative study of atmospheric water-soluble organic aerosols composition in contrasting suburban environments in the Iberian Peninsula Coast, Sci. Total Environ., 648, 430–441, https://doi.org/10.1016/j.scitotenv.2018.08.171, 2019.

Eatough, D. J., Wadsworth, A., Eatough, D. A., Crawford, J. W., Hansen, L. D., and Lewis, E. A.: A multiple-system, multi-channel diffusion denuder sampler for the determination of fine-particulate organic material in the atmosphere, Atmos. Environ. A-Gen., 27, 1213–1219, https://doi.org/10.1016/0960-1686(93)90247-V, 1993.

Farmer, D., and Kreidenweis, S.: HR-ToF-AMS Fine-Mode Aerosol Composition Data, Version 1.0, UCAR/NCAR – Earth Observing Laboratory [data set], https://doi.org/10.26023/MM2Y-ZGFQ-RB0B, 2019.

Finessi, E., Decesari, S., Paglione, M., Giulianelli, L., Carbone, C., Gilardoni, S., Fuzzi, S., Saarikoski, S., Raatikainen, T., Hillamo, R., Allan, J., Mentel, Th. F., Tiitta, P., Laaksonen, A., Petäjä, T., Kulmala, M., Worsnop, D. R., and Facchini, M. C.: Determination of the biogenic secondary organic aerosol fraction in the boreal forest by NMR spectroscopy, Atmos. Chem. Phys., 12, 941–959, https://doi.org/10.5194/acp-12-941-2012, 2012.

Ford, B., Val Martin, M., Zelasky, S. E., Fischer, E. V., Anenberg, S. C., Heald, C. L., and Pierce, J. R.: Future Fire Impacts on Smoke Concentrations, Visibility, and Health in the Contiguous United States, GeoHealth, 2, 229–247, https://doi.org/10.1029/2018gh000144, 2018.

Forrister, H., Liu, J., Scheuer, E., Dibb, J., Ziemba, L., Thornhill, K. L., Anderson, B., Diskin, G., Perring, A. E., Schwarz, J. P., Campuzano-Jost, P., Day, D. A., Palm, B. B., Jose, Jimenez, L., Nenes, A., and Weber, R. J.: Evolution of brown carbon in wildfire plumes, Geophys. Res. Lett., 42, 4623–4630, https://doi.org/10.1002/2015GL063897, 2015.

Foster, K., Pokhrel, R., Burkhart, M., and Murphy, S.: A novel approach to calibrating a photoacoustic absorption spectrometer using polydisperse absorbing aerosol, Atmos. Meas. Tech., 12, 3351–3363, https://doi.org/10.5194/amt-12-3351-2019, 2019.

Fuller, K. A. and Kreidenweis, S. M.: Effects of mixing on extinction by carbonaceous particles, J. Geophys. Res., 104, 15941–15954, https://doi.org/10.1029/1998JD100069, 1999.

Garofalo, L. A., Pothier, M. A., Levin, E. J. T., Campos, T., Kreidenweis, S. M., and Farmer, D. K.: Emission and Evolution of Submicron Organic Aerosol in Smoke from Wildfires in the Western United States, ACS Earth Sp. Chem., 3, 1237–1247, https://doi.org/10.1021/acsearthspacechem.9b00125, 2019.

Gouw, J. A. De, Middlebrook, A. M., Warneke, C., Goldan, P. D., Kuster, W. C., Roberts, J. M., Fehsenfeld, F. C., Worsnop, D. R., Canagaratna, M. R., Pszenny, A. A. P., Keene, W. C., Marchewka, M., Bertman, S. B., and Bates, T. S.: Budget of organic carbon in a polluted atmosphere: Results from the New England Air Quality Study in 2002, J. Geophys. Res., 110, 1–22, https://doi.org/10.1029/2004JD005623, 2005.

Healy, R. M., Wang, J. M., Jeong, C. H., Lee, A. K. Y., Willis, M. D., Jaroudi, E., Zimmerman, N., Hilker, N., Murphy, M., Eckhardt, S., Stohl, A., Abbatt, J. P. D., Wenger, J. C., and Evans, G. J.: Light-absorbing properties of ambient black carbon and brown carbon from fossil fuel and biomass burning sources, J. Geophys. Res.-Atmos., 120, 6619–6633, https://doi.org/10.1002/2015JD023382, 2015.

Hecobian, A., Zhang, X., Zheng, M., Frank, N., Edgerton, E. S., and Weber, R. J.: Water-Soluble Organic Aerosol material and the light-absorption characteristics of aqueous extracts measured over the Southeastern United States, Atmos. Chem. Phys., 10, 5965–5977, https://doi.org/10.5194/acp-10-5965-2010, 2010.

Hu, L. and Permar, W.: PTR-ToF-MS Measurements of Selected NMVOCs Data, Version 3.0, UCAR/NCAR – Earth Observing Laboratory [data set], https://doi.org/10.26023/K9F4-2CNH-EQ0W, 2020.

Hurteau, M. D., Westerling, A. L., Wiedinmyer, C., and Bryant, B. P.: Projected effects of climate and development on California wildfire emissions through 2100, Environ. Sci. Technol., 48, 2298–2304, https://doi.org/10.1021/es4050133, 2014.

Kelesidis, G. A., Neubauer, D., Fan, L. S., Lohmann, U., and Pratsinis, S. E.: Enhanced Light Absorption and Radiative Forcing by Black Carbon Agglomerates, Environ. Sci. Technol., 56, 8610–8618, https://doi.org/10.1021/acs.est.2c00428, 2022.

Kirchstetter, T. W., Novakov, T., and Hobbs, P. V.: Evidence that the spectral dependence of light absorption by aerosols is affected by organic carbon, J. Geophys. Res.-Atmos., 109, 1–12, https://doi.org/10.1029/2004JD004999, 2004.

Kleinman, L. I., Sedlacek III, A. J., Adachi, K., Buseck, P. R., Collier, S., Dubey, M. K., Hodshire, A. L., Lewis, E., Onasch, T. B., Pierce, J. R., Shilling, J., Springston, S. R., Wang, J., Zhang, Q., Zhou, S., and Yokelson, R. J.: Rapid evolution of aerosol particles and their optical properties downwind of wild-

fires in the western US, Atmos. Chem. Phys., 20, 13319–13341, https://doi.org/10.5194/acp-20-13319-2020, 2020.

Krasowsky, T. S., McMeeking, G. R., Wang, D., Sioutas, C., and Ban-Weiss, G. A.: Measurements of the impact of atmospheric aging on physical and optical properties of ambient black carbon particles in Los Angeles, Atmos. Environ., 142, 496–504, https://doi.org/10.1016/j.atmosenv.2016.08.010, 2016.

Lack, D. A. and Cappa, C. D.: Impact of brown and clear carbon on light absorption enhancement, single scatter albedo and absorption wavelength dependence of black carbon, Atmos. Chem. Phys., 10, 4207–4220, https://doi.org/10.5194/acp-10-4207-2010, 2010.

Lack, D. A., Lovejoy, E. R., Baynard, T., Pettersson, A., and Ravishankara, A. R.: Aerosol Absorption Measurement using Photoacoustic Spectroscopy: Sensitivity, Calibration, and Uncertainty Developments, Aerosol Sci. Tech., 40, 697–708, https://doi.org/10.1080/02786820600803917, 2006.

Lack, D. A., Langridge, J. M., Bahreini, R., Cappa, C. D., Middlebrook, A. M., and Schwarz, J. P.: Brown carbon and internal mixing in biomass burning particles, P. Natl. Acad. Sci. USA, 109, 14802–14807, https://doi.org/10.1073/pnas.1206575109, 2012a.

Lack, D. A., Richardson, M. S., Law, D., Langridge, J. M., Cappa, C. D., McLaughlin, R. J., and Murphy, D. M.: Aircraft Instrument for Comprehensive Characterization of Aerosol Optical Properties, Part 2: Black and Brown Carbon Absorption and Absorption Enhancement Measured with Photo Acoustic Spectroscopy, Aerosol Sci. Tech., 46, 555–568, https://doi.org/10.1080/02786826.2011.645955, 2012b.

Levin, E.: Single Particle Soot Photometer (SP2) Black Carbon Mass in Individual Particles Data, Version 2.0, UCAR/NCAR – Earth Observing Laboratory [data set], https://doi.org/10.26023/P8R2-RAB6-N814, 2019.

Lindaas, J., Pollack, I. B., Garofalo, L. A., Pothier, M. A., Farmer, D. K., Kreidenweis, S. M., Campos, T. L., Flocke, F., Weinheimer, A. J., Montzka, D. D., Tyndall, G. S., Palm, B. B., Peng, Q., Thornton, J. A., Permar, W., Wielgasz, C., Hu, L., Ottmar, R. D., Restaino, J. C., Hudak, A. T., Ku, I. T., Zhou, Y., Sive, B. C., Sullivan, A., Collett, J. L., and Fischer, E. V.: Emissions of Reactive Nitrogen From Western U.S. Wildfires During Summer 2018, J. Geophys. Res.-Atmos., 126, 1–21, https://doi.org/10.1029/2020JD032657, 2021.

Liu, D., Whitehead, J., Alfarra, M. R., Reyes-villegas, E., Spracklen, D. V, Reddington, C. L., Kong, S., Williams, P. I., Ting, Y., Haslett, S., Taylor, J. W., Flynn, M. J., Morgan, W. T., Mcfiggans, G., Coe, H., and Allan, J. D.: Black-carbon absorption enhancement in the atmosphere determined by particle mixing state, Nat. Geosci., 10, 184–188, https://doi.org/10.1038/NGEO2901, 2017.

Liu, D., He, C., Schwarz, J. P., and Wang, X.: Lifecycle of light-absorbing carbonaceous aerosols in the atmosphere, npj Clim. Atmos. Sci., 3, 1–18, https://doi.org/10.1038/s41612-020-00145-8, 2020.

Liu, J., Bergin, M., Guo, H., King, L., Kotra, N., Edgerton, E., and Weber, R. J.: Size-resolved measurements of brown carbon in water and methanol extracts and estimates of their contribution to ambient fine-particle light absorption, Atmos. Chem. Phys., 13, 12389–12404, https://doi.org/10.5194/acp-13-12389-2013, 2013.

Liu, S., Aiken, A. C., Gorkowski, K., Dubey, M. K., Cappa, C. D., Williams, L. R., Herndon, S. C., Massoli, P., Fortner, E. C., Chhabra, P. S., Brooks, W. A., Onasch, T. B., Jayne, J. T., Worsnop, D. R., China, S., Sharma, N., Mazzoleni, C., Xu, L., Ng, N. L., Liu, D., Allan, J. D., Lee, J. D., Fleming, Z. L., Mohr, C., Zotter, P., Szidat, S., and Prévôt, A. S. H.: Enhanced light absorption by mixed source black and brown carbon particles in UK winter, Nat. Commun., 6, 8435, https://doi.org/10.1038/ncomms9435, 2015.

Marple, V. A., Rubow, K. L., and Behm, S. M.: A microorifice uniform deposit impactor (moudi): Description, calibration, and use, Aerosol Sci. Tech., 14, 434–436, https://doi.org/10.1080/02786829108959504, 1991.

McClure, C. D., Lim, C. Y., Hagan, D. H., Kroll, J. H., and Cappa, C. D.: Biomass-burning-derived particles from a wide variety of fuels – Part 1: Properties of primary particles, Atmos. Chem. Phys., 20, 1531–1547, https://doi.org/10.5194/acp-20-1531-2020, 2020.

McConnell, J. R., Edwards, R., Kok, L. G., Flanner, M. G., Zender, C. S., Saltzman, E. S., Banta, J. R., Pasteris, D. R., Carter, M. M., and Kahl, J. D. W.: 20th-Century Industrial Black Carbon Emissions Altered Arctic Climate Forcing, Science, 317, 1381–1384, https://doi.org/10.1126/science.1144856, 2007.

Moharreri, A., Craig, L., Dubey, P., Rogers, D. C., and Dhaniyala, S.: Aircraft testing of the new Blunt-body Aerosol Sampler (BASE), Atmos. Meas. Tech., 7, 3085–3093, https://doi.org/10.5194/amt-7-3085-2014, 2014.

Murphy, S.: Aerosol Extinction, Scattering and Absorption (PAS CAPS) Data, Version 1.0, UCAR/NCAR – Earth Observing Laboratory [data set], https://doi.org/10.26023/K8P0-X4T3-TN06, 2019.

Neumann, J. E., Amend, M., Anenberg, S., Kinney, P. L., Sarofim, M., Martinich, J., Lukens, J., Xu, J. W., and Roman, H.: Estimating $PM_{2.5}$-related premature mortality and morbidity associated with future wildfire emissions in the western US, Environ. Res. Lett., 16, 035019, https://doi.org/10.1088/1748-9326/abe82b, 2021.

Onasch, T. B., Massoli, P., Kebabian, P. L., Hills, F. B., Bacon, F. W., and Freedman, A.: Single scattering albedo monitor for airborne particulates, Aerosol Sci. Tech., 49, 267–279, https://doi.org/10.1080/02786826.2015.1022248, 2015.

Orsini, D. A., Ma, Y., Sullivan, A., Sierau, B., Baumann, K., and Weber, R. J.: Refinements to the particle-into-liquid sampler (PILS) for ground and airborne measurements of water soluble aerosol composition, Atmos. Environ., 37, 1243–1259, https://doi.org/10.1016/S1352-2310(02)01015-4, 2003.

Palm, B. B., Peng, Q., Fredrickson, C. D., Lee, B. H., Garofalo, L. A., Pothier, M. A., Kreidenweis, S. M., Farmer, D. K., Pokhrel, R. P., Shen, Y., Murphy, S. M., Permar, W., Hu, L., Campos, T. L., Hall, S. R., Ullmann, K., Zhang, X., Flocke, F., Fischer, E. V., and Thornton, J. A.: Quantification of organic aerosol and brown carbon evolution in fresh wildfire plumes, P. Natl. Acad. Sci. USA, 117, 29469–29477, https://doi.org/10.1073/pnas.2012218117, 2020.

Peltier, R. E., Weber, R. J., and Sullivan, A. P.: Investigating a liquid-based method for online organic carbon detection in atmospheric particles, Aerosol Sci. Tech., 41, 1117–1127, https://doi.org/10.1080/02786820701777465, 2007.

Peng, J., Hu, M., Guo, S., Du, Z., Zheng, J., Shang, D., Zamora, M. L., Zeng, L., Shao, M., Wu, Y. S., Zheng, J., Wang, Y., Glen, C. R., Collins, D. R., Molina, M. J., and Zhang, R.: Markedly enhanced absorption and direct radiative forcing of black carbon under polluted urban environments, P. Natl. Acad. Sci. USA, 113, 4266–4271, https://doi.org/10.1073/pnas.1602310113, 2016.

Peng, Q., Palm, B. B., Melander, K. E., Lee, B. H., Hall, S. R., Ullmann, K., Campos, T., Weinheimer, A. J., Apel, E. C., Hornbrook, R. S., Hills, A. J., Montzka, D. D., Flocke, F., Hu, L., Permar, W., Wielgasz, C., Lindaas, J., Pollack, I. B., Fischer, E. V, Bertram, T. H., and Thornton, J. A.: HONO Emissions from Western U.S. Wildfires Provide Dominant Radical Source in Fresh Wildfire Smoke, Environ. Sci. Technol., 54, 5954–5963, https://doi.org/10.1021/acs.est.0c00126, 2020.

Permar, W., Wang, Q., Selimovic, V., Wielgasz, C., Yokelson, R. J., Hornbrook, R. S., Hills, A. J., Apel, E. C., Ku, I. T., Zhou, Y., Sive, B. C., Sullivan, A. P., Collett, J. L., Campos, T. L., Palm, B. B., Peng, Q., Thornton, J. A., Garofalo, L. A., Farmer, D. K., Kreidenweis, S. M., Levin, E. J. T., DeMott, P. J., Flocke, F., Fischer, E. V., and Hu, L.: Emissions of Trace Organic Gases From Western U.S. Wildfires Based on WE-CAN Aircraft Measurements, J. Geophys. Res.-Atmos., 126, 1–29, https://doi.org/10.1029/2020JD033838, 2021.

Pokhrel, R. P., Beamesderfer, E. R., Wagner, N. L., Langridge, J. M., Lack, D. A., Jayarathne, T., Stone, E. A., Stockwell, C. E., Yokelson, R. J., and Murphy, S. M.: Relative importance of black carbon, brown carbon, and absorption enhancement from clear coatings in biomass burning emissions, Atmos. Chem. Phys., 17, 5063–5078, https://doi.org/10.5194/acp-17-5063-2017, 2017.

Romshoo, B., Müller, T., Pfeifer, S., Saturno, J., Nowak, A., Ciupek, K., Quincey, P., and Wiedensohler, A.: Optical properties of coated black carbon aggregates: numerical simulations, radiative forcing estimates, and size-resolved parameterization scheme, Atmos. Chem. Phys., 21, 12989–13010, https://doi.org/10.5194/acp-21-12989-2021, 2021.

Saleh, R.: From Measurements to Models: Toward Accurate Representation of Brown Carbon in Climate Calculations, Curr. Pollut. Reports, 6, 90–104, https://doi.org/10.1007/s40726-020-00139-3, 2020.

Saleh, R., Robinson, E. S., Tkacik, D. S., Ahern, A. T., Liu, S., Aiken, A. C., Sullivan, R. C., Presto, A. A., Dubey, M. K., Yokelson, R. J., Donahue, N. M., and Robinson, A. L.: Brownness of organics in aerosols from biomass burning linked to their black carbon content, Nat. Geosci., 7, 647–650, https://doi.org/10.1038/ngeo2220, 2014.

Sarangi, C., Qian, Y., Rittger, K., Leung, R. L., Chand, D., Bormann, K. J., and Painter, T. H.: Dust dominates high-altitude snow darkening and melt over high-mountain Asia, Nat. Clim. Chang., 10, 1045–1051, https://doi.org/10.1038/s41558-020-00909-3, 2020.

Schnaiter, M., Horvath, H., Möhler, O., Naumann, K. H., Saathoff, H., and Schöck, O. W.: UV-VIS-NIR spectral optical properties of soot and soot-containing aerosols, J. Aerosol Sci., 34, 1421–1444, https://doi.org/10.1016/S0021-8502(03)00361-6, 2003.

Schnaiter, M., Linke, C., Möhler, O., Naumann, K. H., Saathoff, H., Wagner, R., Schurath, U., and Wehner, B.: Absorption amplification of black carbon internally mixed with secondary organic aerosol, J. Geophys. Res.-Atmos., 110, 1–11, https://doi.org/10.1029/2005JD006046, 2005.

Schwarz, J. P., Gao, R. S., Fahey, D. W., Thomson, D. S., Watts, L. A., Wilson, J. C., Reeves, J. M., Darbeheshti, M., Baumgardner, D. G., Kok, G. L., Chung, S. H., Schulz, M., Hendricks, J., Lauer, A., Ka, B., Slowik, J. G., Rosenlof, K. H., Thompson, T. L., Langford, A. O., Loewenstein, M., and Aikin, K. C.: Single-particle measurements of midlatitude black carbon and light-scattering aerosols from the boundary layer to the lower stratosphere, J. Geophys. Res., 111, D16207, https://doi.org/10.1029/2006JD007076, 2006.

Sedlacek, A. and Lee, J.: Photothermal interferometric aerosol absorption spectrometry, Aerosol Sci. Tech., 41, 1089–1101, https://doi.org/10.1080/02786820701697812, 2007.

Subramanian, R., Kok, G. L., Baumgardner, D., Clarke, A., Shinozuka, Y., Campos, T. L., Heizer, C. G., Stephens, B. B., de Foy, B., Voss, P. B., and Zaveri, R. A.: Black carbon over Mexico: the effect of atmospheric transport on mixing state, mass absorption cross-section, and BC/CO ratios, Atmos. Chem. Phys., 10, 219–237, https://doi.org/10.5194/acp-10-219-2010, 2010.

Sullivan, A.: Particle Into Liquid Sampler 1 (PILS1) Three second integrated WSOC Data, Version 1.0, UCAR/NCAR – Earth Observing Laboratory [data set], https://doi.org/10.26023/9H07-MD9K-430D, 2019.

Sullivan, A.: Particle Into Liquid Sampler 1 (PILS1) Sixteen second integrated Abs365, Version 2.0, UCAR/NCAR – Earth Observing Laboratory [data set], https://doi.org/10.26023/CRHY-NDT9-C30V, 2021a.

Sullivan, A.: Particle Into Liquid Sampler 2 (PILS2) two minute integrated cations, anions, levoglucosan, and organic acids data, Version 1.0, UCAR/NCAR – Earth Observing Laboratory [data set], https://doi.org/10.26023/7TAN-TZMD-680Y, 2021b.

Sullivan, A. P., Pokhrel, R. P., Shen, Y., Murphy, S. M., Toohey, D. W., Campos, T., Lindaas, J., Fischer, E. V., and Collett Jr., J. L.: Examination of brown carbon absorption from wildfires in the western US during the WE-CAN study, Atmos. Chem. Phys., 22, 13389–13406, https://doi.org/10.5194/acp-22-13389-2022, 2022.

Sun, Y., Zhang, Q., Zheng, M., Ding, X., Edgerton, E. S., and Wang, X.: Characterization and source apportionment of water-soluble organic matter in atmospheric fine particles ($PM_{2.5}$) with high-resolution aerosol mass spectrometry and GC-MS, Environ. Sci. Technol., 45, 4854–4861, https://doi.org/10.1021/es200162h, 2011.

Taylor, J. W., Wu, H., Szpek, K., Bower, K., Crawford, I., Flynn, M. J., Williams, P. I., Dorsey, J., Langridge, J. M., Cotterell, M. I., Fox, C., Davies, N. W., Haywood, J. M., and Coe, H.: Absorption closure in highly aged biomass burning smoke, Atmos. Chem. Phys., 20, 11201–11221, https://doi.org/10.5194/acp-20-11201-2020, 2020.

Toohey, D.: CVI/UHSAS Data, Version 1.1, UCAR/NCAR – Earth Observing Laboratory [data set], https://doi.org/10.26023/BZ4F-EAC4-290W, 2019.

Wang, X., Heald, C. L., Sedlacek, A. J., de Sá, S. S., Martin, S. T., Alexander, M. L., Watson, T. B., Aiken, A. C., Springston, S. R., and Artaxo, P.: Deriving brown carbon from multiwavelength absorption measurements: method and application to AERONET and Aethalometer observations, Atmos. Chem. Phys., 16, 12733–12752, https://doi.org/10.5194/acp-16-12733-2016, 2016.

Wang, X., Heald, C. L., Liu, J., Weber, R. J., Campuzano-Jost, P., Jimenez, J. L., Schwarz, J. P., and Perring, A. E.: Exploring the

observational constraints on the simulation of brown carbon, Atmos. Chem. Phys., 18, 635–653, https://doi.org/10.5194/acp-18-635-2018, 2018.

Wei, Y., Ma, L., Cao, T., Zhang, Q., Wu, J., Buseck, P. R., and Thompson, J. E.: Light scattering and extinction measurements combined with laser-induced incandescence for the real-time determination of soot mass absorption cross section, Anal. Chem., 85, 9181–9188, https://doi.org/10.1021/ac401901b, 2013.

Westerling, A. L., Hidalgo, H. G., Cayan, D. R., and Swetnam, T. W.: Warming and Earlier Spring Increase Western U. S. Forest Wildfire Activity, Science, 313, 940–943, https://doi.org/10.1126/science.1128834, 2006.

Williams, E. L. and Grosjean, D.: Removal of Atmospheric Oxidants with Annular Denuders, Environ. Sci. Technol., 24, 811–814, https://doi.org/10.1021/es00076a002, 1990.

Wonaschütz, A., Hitzenberger, R., Bauer, H., Pouresmaeil, P., Klatzer, B., Caseiro, A., and Puxbaum, H.: Application of the integrating sphere method to separate the contributions of brown and black carbon in atmospheric aerosols, Environ. Sci. Technol., 43, 1141–1146, https://doi.org/10.1021/es8008503, 2009.

Yue, X., Mickley, L. J., Logan, J. A., and Kaplan, J. O.: Ensemble projections of wildfire activity and carbonaceous aerosol concentrations over the western United States in the mid-21st century, Atmos. Environ., 77, 767–780, https://doi.org/10.1016/j.atmosenv.2013.06.003, 2013.

Zeng, L., Zhang, A., Wang, Y., Wagner, N. L., Katich, J. M., Schwarz, J. P., Schill, G. P., Brock, C., Froyd, K. D., Murphy, D. M., Williamson, C. J., Kupc, A., Scheuer, E., Dibb, J., and Weber, R. J.: Global Measurements of Brown Carbon and Estimated Direct Radiative Effects, Geophys. Res. Lett., 47, 1–11, https://doi.org/10.1029/2020GL088747, 2020.

Zeng, L., Sullivan, A. P., Washenfelder, R. A., Dibb, J., Scheuer, E., Campos, T. L., Katich, J. M., Levin, E., Robinson, M. A., and Weber, R. J.: Assessment of online water-soluble brown carbon measuring systems for aircraft sampling, Atmos. Meas. Tech., 14, 6357–6378, https://doi.org/10.5194/amt-14-6357-2021, 2021.

Zeng, L., Dibb, J., Scheuer, E., Katich, J. M., Schwarz, J. P., Bourgeois, I., Peischl, J., Ryerson, T., Warneke, C., Perring, A. E., Diskin, G. S., DiGangi, J. P., Nowak, J. B., Moore, R. H., Wiggins, E. B., Pagonis, D., Guo, H., Campuzano-Jost, P., Jimenez, J. L., Xu, L., and Weber, R. J.: Characteristics and evolution of brown carbon in western United States wildfires, Atmos. Chem. Phys., 22, 8009–8036, https://doi.org/10.5194/acp-22-8009-2022, 2022.

Zhang, L., Segal-Rozenhaimer, M., Che, H., Dang, C., Sedlacek III, A. J., Lewis, E. R., Dobracki, A., Wong, J. P. S., Formenti, P., Howell, S. G., and Nenes, A.: Light absorption by brown carbon over the South-East Atlantic Ocean, Atmos. Chem. Phys., 22, 9199–9213, https://doi.org/10.5194/acp-22-9199-2022, 2022.

Zhang, Y., Forrister, H., Liu, J., DIbb, J., Anderson, B., Schwarz, J. P., Perring, A. E., Jimenez, J. L., Campuzano-Jost, P., Wang, Y., Nenes, A., and Weber, R. J.: Top-of-atmosphere radiative forcing affected by brown carbon in the upper troposphere, Nat. Geosci., 10, 486–489, https://doi.org/10.1038/ngeo2960, 2017.